NOAA TR ERL 322-WPL 38

Quantitative Evaluation of Acoustic Echoes from the Planetary Boundary Layer

WILLIAM D. NEFF

U.S. DEPARTMENT OF COMMERCE
NATIONAL OCEANIC AND ATMOSPHERIC ADMINISTRATION
ENVIRONMENTAL RESEARCH LABORATORIES
TECHNICAL REPORT BOULDER, COLORADO

JUNE 1975

NOAA TECHNICAL REPORT ERL 322-WPL 38

U.S. DEPARTMENT OF COMMERCE
Rogers C.B. Morton, Secretary
NATIONAL OCEANIC AND ATMOSPHERIC ADMINISTRATION
Robert M. White, Administrator
ENVIRONMENTAL RESEARCH LABORATORIES
Wilmot N. Hess, Director

QUANTITATIVE EVALUATION OF ACOUSTIC ECHOES FROM THE PLANETARY BOUNDARY LAYER

WILLIAM D. NEFF

BOULDER, COLORADO JUNE 1975

For sale by the Superintendent of Documents, U.S. Government Printing Office,
Washington, D.C. 20402

Table of Contents

Abstract

Using two acoustic echosounders (echosondes), one of which operated at stimultaneous wavelengths of 0.12, 0.15, and 0.19 m, the acoustic backscatter cross section was obtained as a function of time and height in the planetary boundary layer. The cross sections were interpreted in terms of the temperature structure parameter C_T^2 and compared with values obtained *in situ* at the 92-m level on a tower located some 300 m distant. In general, excellent agreement was found between the two sets of C_T^2 values under statically unstable conditions. Under statically stable conditions, the measurements, on occasion, disagreed by factors ranging from 2 to 5 with the echo-derived C_T^2 values consistently overestimating those from the tower. Our analysis suggested that the errors were due to the different spatial-sampling characteristics of the two techniques rather than a lack of isotropy and homogeneity at small scales.

1. Introduction

Acoustic echo sounding[1] and microwave radar techniques portray in detail the larger scale features of the planetary boundary layer (Beran et al., 1973; Gossard et al., 1971; Ottersten et al., 1973). Small-scale refractive index fluctuations provide tracers for both techniques. These fluctuations usually arise when turbulence occurs within a region of refractive index gradient, associated for example with temperature inversion layers or convection regions produced by surface heating. This report describes redundant and multiwavelength measurement of the acoustic backscatter from such small-scale structures.

A scattering cross-section calculation, using a temperature spectrum approach, provides a useful quantitative interpretation of acoustic echoes (Tatarskii, 1961, 1971; Little, 1969). Using such an analysis, we compare echosonde-derived and *in situ* values of the temperature structure parameter C_T^2 (to be defined below) for several time periods. These periods include the transition from turbulence dominated by static stability to that arising from static instability. We carry out this analysis from two aspects: First, we examine the longer term statistics in the form of cumulative probability distributions, averaged vertical profiles, and time series of C_T^2 from each source. This provides a test of several theoretical predictions. Second, finding occasional discrepancies, we examine the correlation of short-term features, such as shear instability events, over the tower-echosonde separation (300 m). This gives additional insight into the spatial distribution of small-scale turbulence under statically stable conditions and suggests that the source of the observed discrepancies lies in the different spatial-averaging characteristics of the two methods.

Table 1 lists the operating parameters for the two echosondes used in our analysis. A discussion of their operation and calibration appears in the appendix. Figure 1 shows the relative location of the 152-m tower for our *in situ* measurements, the echosondes, and a collocated microbarograph array (Hooke et al., 1973). This tower site lies in a shallow bowl, 25 km wide and 75 m deep, on the plains of eastern Colorado near the town of Haswell.

[1]Acoustic echo sounders will be referred to as "echosondes" following recent usage (e.g., E.H. Brown, 1974).

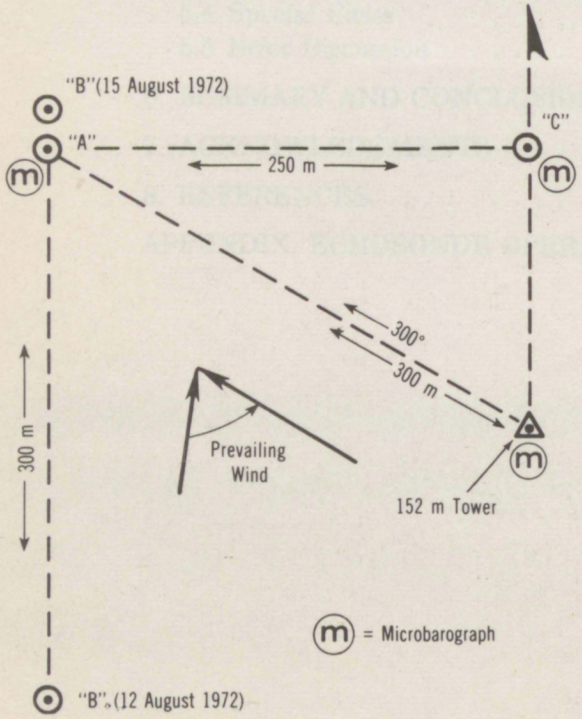

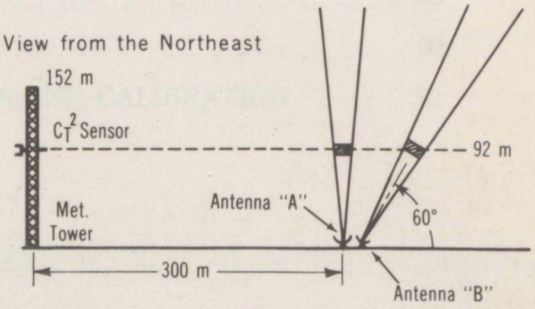

Figure 1. Relative locations of the Haswell meteorological tower, the echosondes, and microbarographs. Antenna A was directed vertically, while Antenna B was tilted 30° from the vertical and directed to the north (for data obtained on 15 August 1972).

2. Theory

2.1 The Echosonde Equation

The monostatic echosonde equation relates the range-gated transducer voltage to the corresponding scattering cross section per unit volume. In terms of measured and/or calculated quantities;

$$\frac{P_R}{E_R} = \left[P_T \cdot E_T\right] \cdot \left[e^{-2\bar{\alpha}R}\right] \cdot \left[\sigma_0(R,f) \cdot \left(\frac{c\tau}{2}\right) \cdot \left(\frac{A}{R^2} \cdot G\right)\right] \quad (1)$$

with $\frac{P_R}{E_R}$ = received power where P_R = measured electrical power and E_R = efficiency of conversion from received acoustic power,

$P_T \cdot E_T$ = radiated power where P_T = electrical power applied to the transducer and E_T = efficiency of conversion to radiated acoustic power,

$e^{-2\bar{\alpha}R}$ = round trip loss of power resulting from attenuation by air where $\bar{\alpha}$ = average attenuation (m^{-1}) to the scattering volume at range R (m),

$\sigma_0(R,f)$ = scattering cross section per unit volume; that is, fraction of incident power backscattered per unit distance into unit solid angle at frequency f,

$c\tau/2$ = maximum effective-scattering volume thickness where c = local speed of sound (ms^{-1}) and τ = pulse length (s), and

$\frac{A}{R^2} \cdot G$ = solid angle subtended by the antenna aperture A (m^2) at range R (m) from the scattering volume, modified by an effective-aperture factor G, arising from the antenna's directivity.

This equation provides σ_0 which we then relate to *in situ* measurements. We assume the validity of this "cross-section-radar-equation" approximation. Wheelon (1972) describes limitations on this approach, but the alternative general formulation lacks the utility of (1). The calculation of the correction terms in (1) is described in the appendix.

Table 1. Echosonde Parameters

Parameter	*Single frequency*	*Multifrequency*
Vertical range	340 or 680 m	294 or 589 m
Frequencies	2250 Hz	1750, 2250, and 2750 Hz
Electrical power	100 W	25 W
Efficiencies	4.5%	4.5%, 4.5%, and 2.8%
Pulse lengths	6, 20, or 30 ms	6, 20, or 30 ms
Band width	100 Hz	100 or 300 Hz
Elevation angle	90°	60°
Azimuth	—	000°
Antenna area	1.8 m^2	1.8 m^2

2.2 Cross Section Interpretation

The theoretical description of wave scattering in a turbulent atmosphere, on which our interpretation of σ_0 depends, has an extensive literature. Batchelor (1957) expresses the scattering cross section in terms of the spectral densities of temperature and turbulent kinetic energy. Kraichnan (1953) and Lighthill (1953) show that velocity fluctuations do not contribute to the backscattered intensity for an isotropic energy spectral density. Tatarskii (1961, 1971) provides a number of useful results that couple the scattering theory with inertial-subrange turbulence results. E. H. Brown (1974) reviews more recent theoretical work.

Tatarskii (1971) expresses the acoustic backscatter cross section per unit volume σ_0, in terms of the isotropic, three-dimensional spectral density of temperature ϕ_T, as

$$\sigma_0 = \frac{\pi}{2} k^4 \frac{\phi_T(2k)}{T_0^2} \tag{2}$$

where $k = 2\pi/\lambda$ is the incident acoustic wavenumber at wavelength λ and T_0 is the local mean temperature. The evaluation of ϕ_T at a wavenumber of $2k$ arises from the in-phase addition of backscattered waves from those inhomogeneities spaced $\lambda/2$ apart along the radial propagation direction. Such temperature inhomogeneities can be characterized by the temperature structure function D_T, defined by

$$D_T(\mathbf{r}) = [(T(\mathbf{x}) - T(\mathbf{x}+\mathbf{r}))^2] \tag{3}$$

where [ ] indicates an ensemble average, $\mathbf{x}$ denotes the location at which D_T is evaluated, and $\mathbf{r}$ is the separation between the sensors. When $|\mathbf{r}|$ lies within the inertial subrange of the temperative fluctuations, dimensional arguments and experimental results (Tatarskii, 1971) show that

$$D_T(r) = C_T^2 r^{2/3} \tag{4}$$

where $r = |\mathbf{r}|$. The constant of proportionality C_T^2 is called the "temperature structure parameter." A connection between D_T and ϕ_T arises from the expression

$$D_T(r) = 8\pi \int_0^\infty \left(1 - \frac{\sin kr}{kr}\right) \phi_T(k) k^2 dk, \tag{5}$$

derived by Tatarskii (1971), which, using (4) and (2), yields the cross section

$$\sigma_0 = 0.0039\, k^{1/3} \frac{C_T^2}{T_0^2}. \tag{6}$$

Using this and the radar equation (1), one obtains a volume-averaged measure of C_T^2 from each echosonde range gate. Our analysis compares these values with those obtained directly from tower sensors using the expressions (3) and (4). Little (1969) outlines the potential usefulness of this kind of analysis in the remote sensing of boundary layer turbulence.

Both echosondes and tower instruments sample the high wavenumber range of ϕ_T. However, the echosonde samples over a narrow band of wavenumbers centered on $2k$ (where the width results from the truncation of the pulse volume). In contrast, the direct structure-function measurement weights the spectrum according to (5) so that the tower-derived values of C_T^2 may reveal a smaller variance (cf., fig. 5). The derivation (Tatarskii, 1971), in addition, ignores the spatial variation of the correlation function over the scattering volume (ϕ_T is the Fourier transform of the two-point correlation function of the temperature fluctuations). This, combined with the spatial intermittancy of the turbulence, may make the variance of the echosonde-derived values of C_T^2 sensitive to the size of the scattering volume.

Electromagnetic and acoustic scattering cross sections have been observed that are much larger than those predicted *in situ* (Metcalf and Atlas, 1973; Beran et al., 1973). Moreover, the power-law dependence in (4) may be modified when the spatial randomness of the kinetic-energy dissipation rate ϵ and the rate of destruction of the temperature fluctuations N, and their possible correlation, are considered (Tennekes, 1973b). This suggests an examination of the sen-

sitivity of our comparisons to the "2/3 power law." We hypothesize that

$$D_T(r)=[(\Delta T)^2]=C_\mu{}^2 r^\mu \tag{7}$$

where ΔT is the temperature difference between sensors spaced a distance r apart. Following Tatarskii (1971), (5) and (7) yield

$$\sigma_0=\frac{k^4}{8\pi T_0{}^2}F(\mu,k)C_\mu{}^2=\frac{k^4}{8\pi T_0{}^2}F(\mu,k)\frac{[(\Delta T)^2]}{r^\mu}$$

where $F(\mu,k)=\Gamma(\mu+2)\sin\left(\frac{\pi\mu}{2}\right)(2k)^{-(\mu+3)}$.

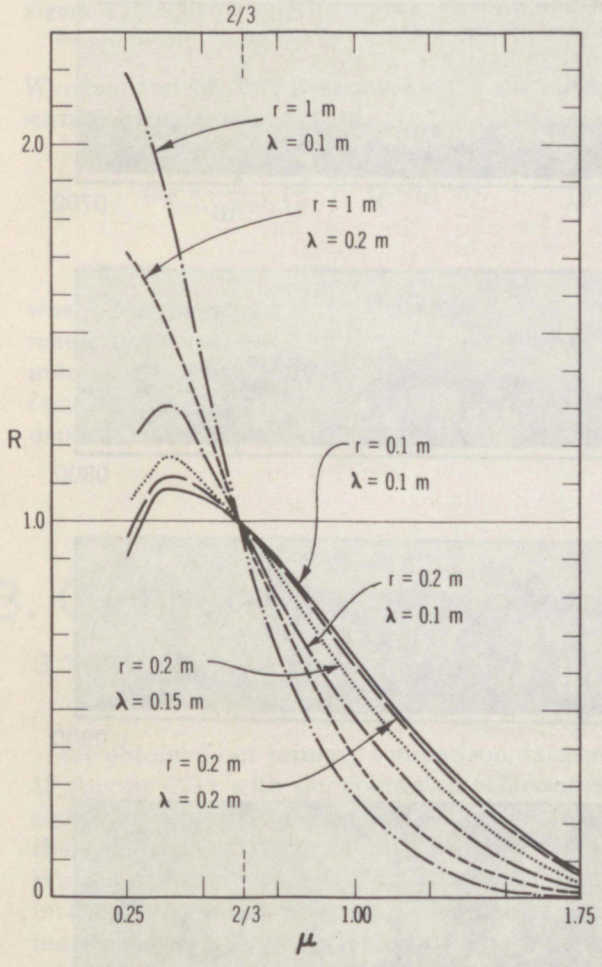

Figure 2. Using the power-law dependence $[(\Delta T)^2] \propto r_\mu$, we have plotted the ratio $R=\sigma(\mu,\lambda)/\sigma(\mu=2/3,\lambda)$ as a function of μ for several values of r and λ (r is the separation of the temperature sensors, λ is the acoustic wavelength, and $\sigma(\mu,\lambda)$ is the acoustic scattering cross section per unit volume).

For a given value of $D_T=[(\Delta T)^2]$, the behavior of σ_0 as a function of μ can be examined relative to a cross section predicted from the "2/3 power law." We form the ratio

$$R=\frac{\sigma_0(\mu)}{\sigma_0(\mu=2/3)}=\frac{F(\mu,k)}{F(2/3,k)}\frac{r^{2/3}}{r^\mu}.$$

This ratio, as a function of μ, is plotted in figure 2 for several values of r and $\lambda=2\pi\ k^{-1}$. This shows that the use of $\mu=2/3$ will predict larger cross sections than will $\mu>2/3$. For $\mu<2/3$ and $r\approx\lambda$, only small variations ($\approx$10%) will result. Thus, larger-than-expected cross sections from the echosonde do not appear directly traceable to a failure of the "2/3 power law."

2.3 Turbulence-Theory Predictions

Inertial-subrange assumptions can be tested indirectly through the form of the cumulative probability distributions. This follows from the relation between $C_T{}^2$ and other meteorological fields that arises when an inertial subrange is assumed. This relation is given by (Tatarskii, 1961; Wyngaard and Coté, 1971)

$$C_T{}^2=3.2\,N\,\epsilon^{-1/3} \tag{8}$$

where N is the rate of destruction of the temperature fluctuations ($°C^2s^{-1}$) through conduction and ϵ is the dissipation rate of turbulent kinetic energy (m^2s^{-3}). Because $ln\ \epsilon$ and $ln\ N$ should possess Gaussian distributions (Oboukhov, 1962; Kolmogorov, 1962; Gurvich

and Yaglom, 1967), it follows that C_T^2 should be similarly distributed with the greatest dependence on N rather than ϵ (Gibson et al., 1970). In general, the apparent lognormality of the echosonde and tower C_T^2 data will also depend on noise levels, electronic saturation, and the number of samples in the distribution. One should also note that such probability distributions will reflect contributions from scales over which the echo intensity and *in situ* data are averaged.

Another method by which the ability of the echosonde to measure C_T^2 can be judged is through the observed height dependence of C_T^2.

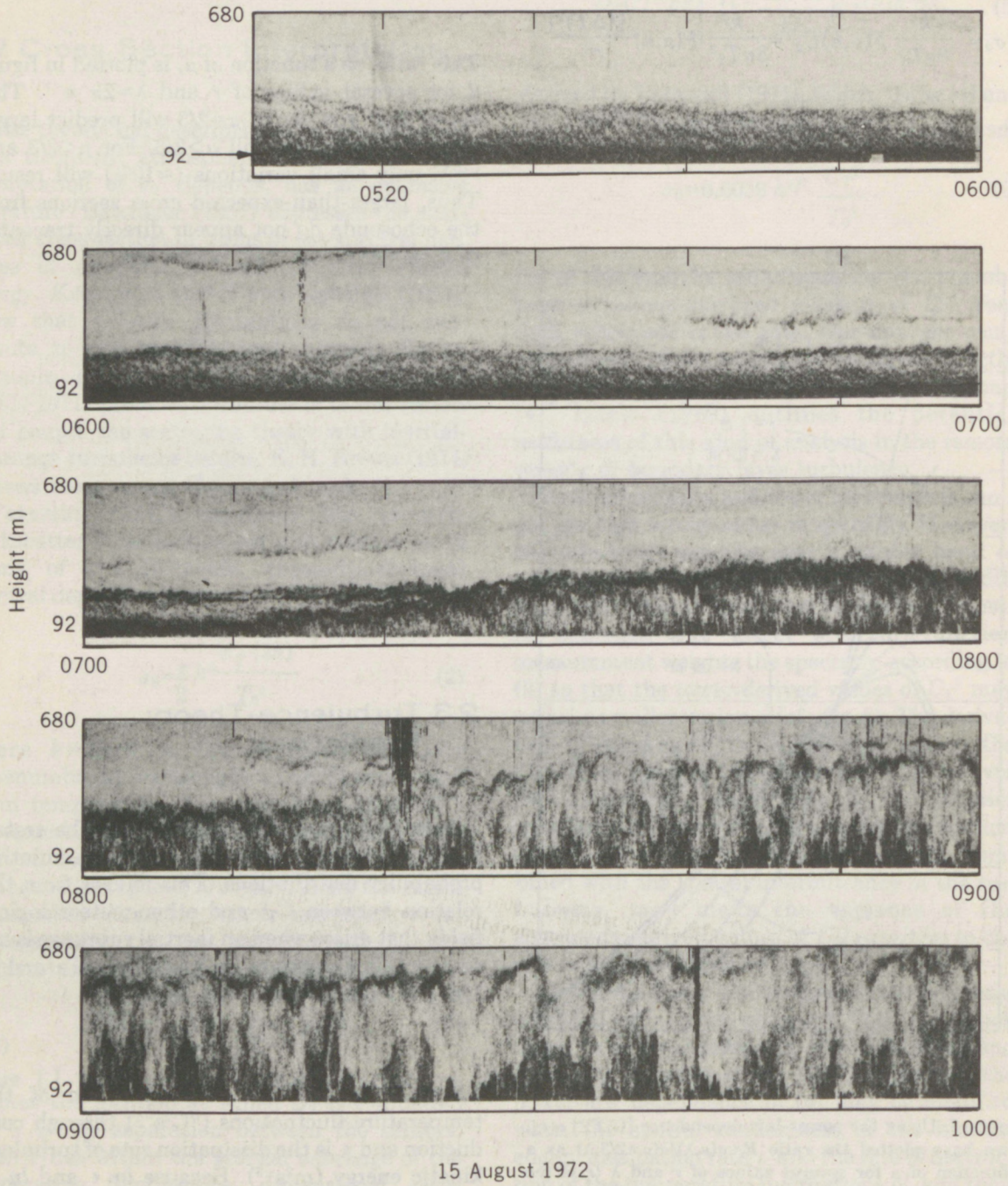

Figure 3. Vertically directed echosonde facsimile record obtained from 0510 to 1000, 15 August 1972, at Haswell. The vertical scale is 680 m. Dark spikes originating at the top of the record result from noise transients.

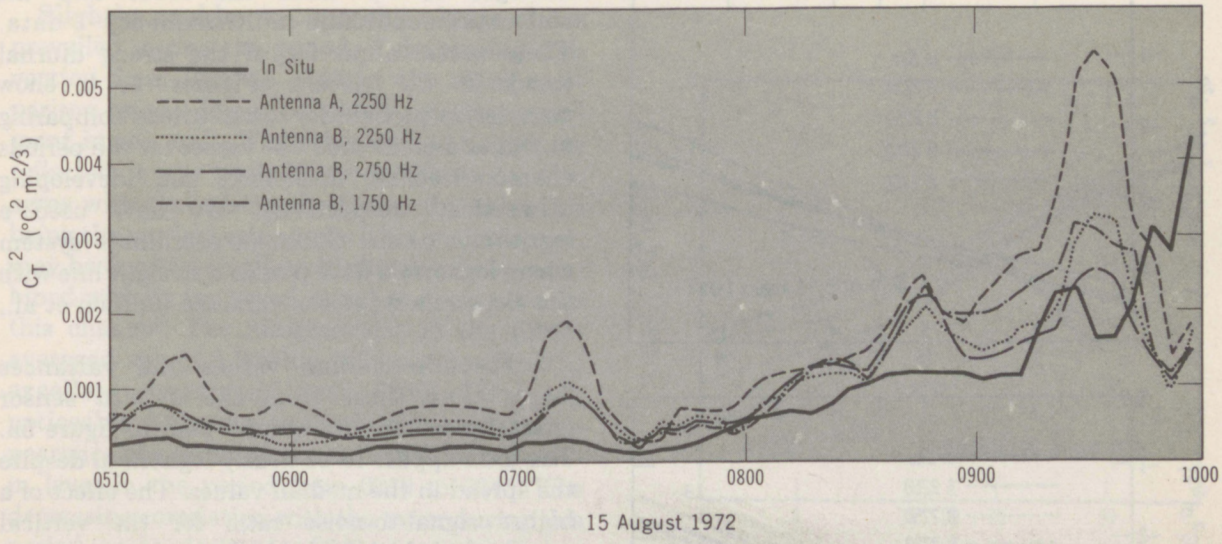

Figure 4. Time series of C_T^2 from each echosonde and the tower, at 92 m above the surface, for the period from 0510 to 1000, 15 August 1972. Data were filtered with a 15-min running average and then averaged in 5-min blocks for plotting.

Wyngaard et al. (1971) shows for the unstable surface boundary layer that

$$C_T^2 = \frac{4}{3K^{2/3}} \left(\frac{\overline{T}}{g}\right)^{2/3} Q_0^{4/3} Z^{-4/3} \qquad (9)$$

where Z is the height above the surface, $\overline{T}$ is the mean temperature, $g = 9.8$ ms^{-2}, K = vonKármán's constant, and $Q_0 = \overline{w'T'}$ which is the surface vertical temperature flux. The height dependence in (9), which is predicated on the existence of free convection, has been observed to hold well beyond the surface layer under unstable conditions (Tsvang, 1969). Measurements obtained in the marine boundary layer indicate that the presence of a capping inversion modifies the height dependence of C_T^2 (Frisch and Ochs, 1975). To test these various predictions, cumulative probability distributions and vertical profiles of C_T^2 were generated. The distributions were obtained over adjacent time periods representing distinct turbulence regimes.

3. C_T^2 Data Comparisons

3.1 15 August Data

We obtained our primary comparison data on 15 August 1972 with the collocated echosondes shown in figure 1. Antenna "B", tilted 30° from the vertical, operated in a multifrequency mode. We averaged the tower C_T^2 data (which had an internal-filter time constant of 1 s) over 4 s, matching the 4-s pulse repetition period of the echosonde. With a nominal 5 ms^{-1} windspeed, this yielded a horizontal spatial average comparable with the beamwidth at 92 m. The mean wind generally lay within 10° to 50° of the tower-echosonde axis. The sensors were located on the windward side of the tower.

A weak nocturnal inversion characterized the early morning period of our analysis. The development of convection and the associated rise of the inversion followed 0700 as shown in the facsimile record (fig. 3). The quasi-stationarity of the inversion height from 0730 to 0820 (indicated roughly by the dark layer at 200 m) reveals the effect of a region of increased static stability. Following 0830, the inversion lifts approximately linearly with time (e.g., Tennekes, 1973a).

Figure 4 shows a time-series comparison of C_T^2 levels (at 92 m) where we have plotted 5-min

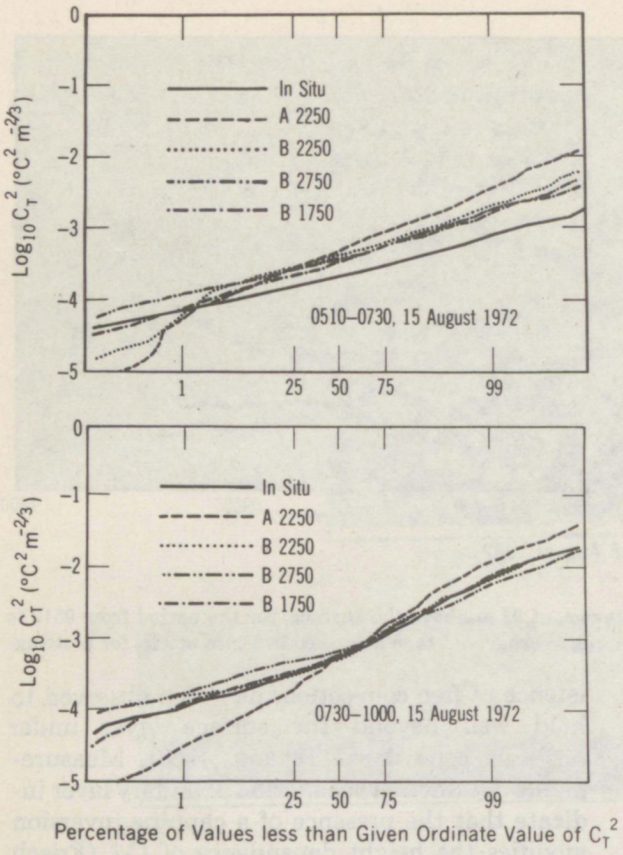

averages of C_T^2 from the tower and the collocated-echosonde-multifrequency data. These reveal a portion of the strong diurnal trend in C_T^2 levels. Figures 5a, b show cumulative probability distributions comparing *in situ* and echosonde C_T^2 values for the periods characterized as "inversion," and "developing convection," respectively. We have used a logrithmic *versus* Gaussian coordinate system where lognormal data plot as a straight line with the slope related to the variance (Gibson et al., 1970).

Echosonde median values and variances larger than those from the *in situ* sensor characterize the "inversion" case in figure 5a. The data appear to be nearly lognormal despite the spread in the median values. The effect of a higher signal-to-noise ratio for the vertical echosonde (which had a higher radiated power) shows clearly in the probability distributions in figure 5. The discrepancy in the median values will be discussed in a later section.

Figure 5. Cumulative probability distributions of C_T^2 obtained from each echosonde and the tower at 92 m. Unfiltered 4-s samples were used in the distributions on 15 August 1972: (a) 0510 to 0730; and (b) 0730 to 1000.

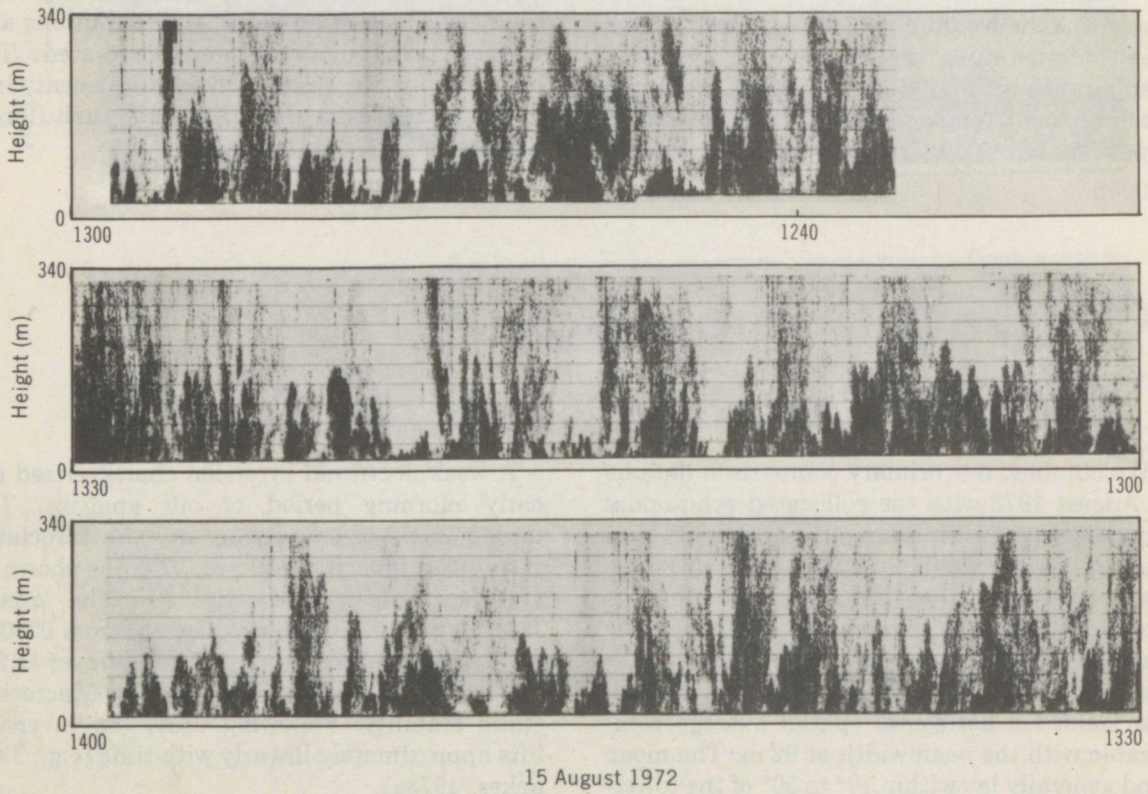

Figure 6. The echosonde facsimile record from 1235 to 1400, 15 August 1972. Vertical range is 340 m. A pulse length of 20 ms and repetition period of 2 s were used.

Slightly stable to unstable lapse rates prevailed during the period of developing convection from 0730 to 1000 at the 92-m comparison height. Figure 5b shows excellent agreement in this case. The echosonde variances, as reflected in the probability distributions, also agree with those from the tower, the exception being the vertical echosonde. This one exception may be due to a small multiplicative error, combined with an improved signal-to-noise ratio in this channel. The disagreement in the block-averaged values following 0900 occurs after the excellent agreement near 0850. The only noticeable difference on the facsimile is the appearance of a series of plume "tops" near the 92-m level in the period from 0910 to 0945. The decreasing correlation with the tower during this period, particularly near 0940, may arise from a local modulation of the convective thermal structure by vortex rolls or other instability modes in the boundary layer flow (e.g., R. A. Brown, 1974; LeMone, 1973).

A period during the early afternoon on 15 August was also analyzed. the facsimile record is shown in figure 6. The echosonde operated with a pulse length of 20 ms and a repetition period of 2 s. The wind was perpendicular to the tower-echosonde axis. The distributions, as shown in figure 7, agree very well for larger values of C_T^2, with the exception of the shift in the 1750-Hz data which can be attributed to a change in transducer efficiency with temperature. The disagreement at the low end of the distributions again results from different noise characteristics for the two echosondes. An apparent bimodality in the distributions appears in the convective

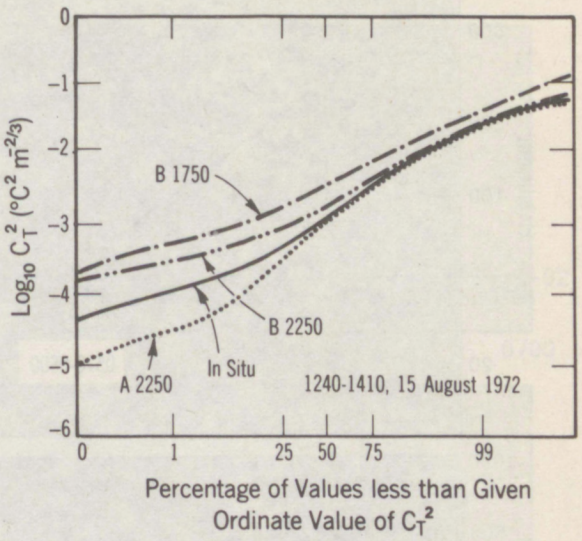

Figure 7. Cumulative probability distributions of C_T^2 obtained from the echosondes and the tower at 92 m. Unfiltered, 2-s samples from the period 1240 to 1400, 15 August 1972, were used.

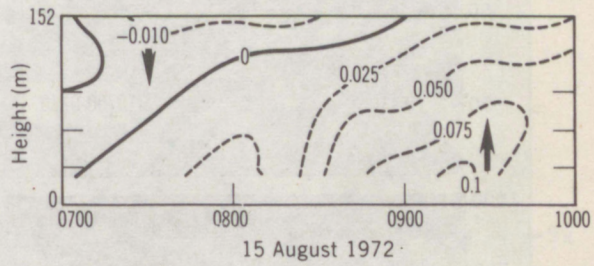

Figure 8. Isopleths of temperature flux $Q=\overline{w'T'}$ (°C ms^{-1}), derived from the fixed-level tower data. Temperature data were detrended using a 20-min running average.

Table 2. Echosonde-Tower Temperature Flux Comparisons From 0730 to 0950, 15 August 1972

Time period	0730-0750	0750-0810	0810-0830	0830-0850	0850-0910	0910-0930	0930-0950
Echosonde surface flux °C ms^{-1}	0.044	0.054	0.067	0.095	0.118	0.141	0.148
Tower 32-m flux	0.018	0.034	0.015	0.064	0.088	0.105	0.075
Height of C_T^2 minimum	130 m	140 m	160 m	250 m	290 m	280 m	330 m

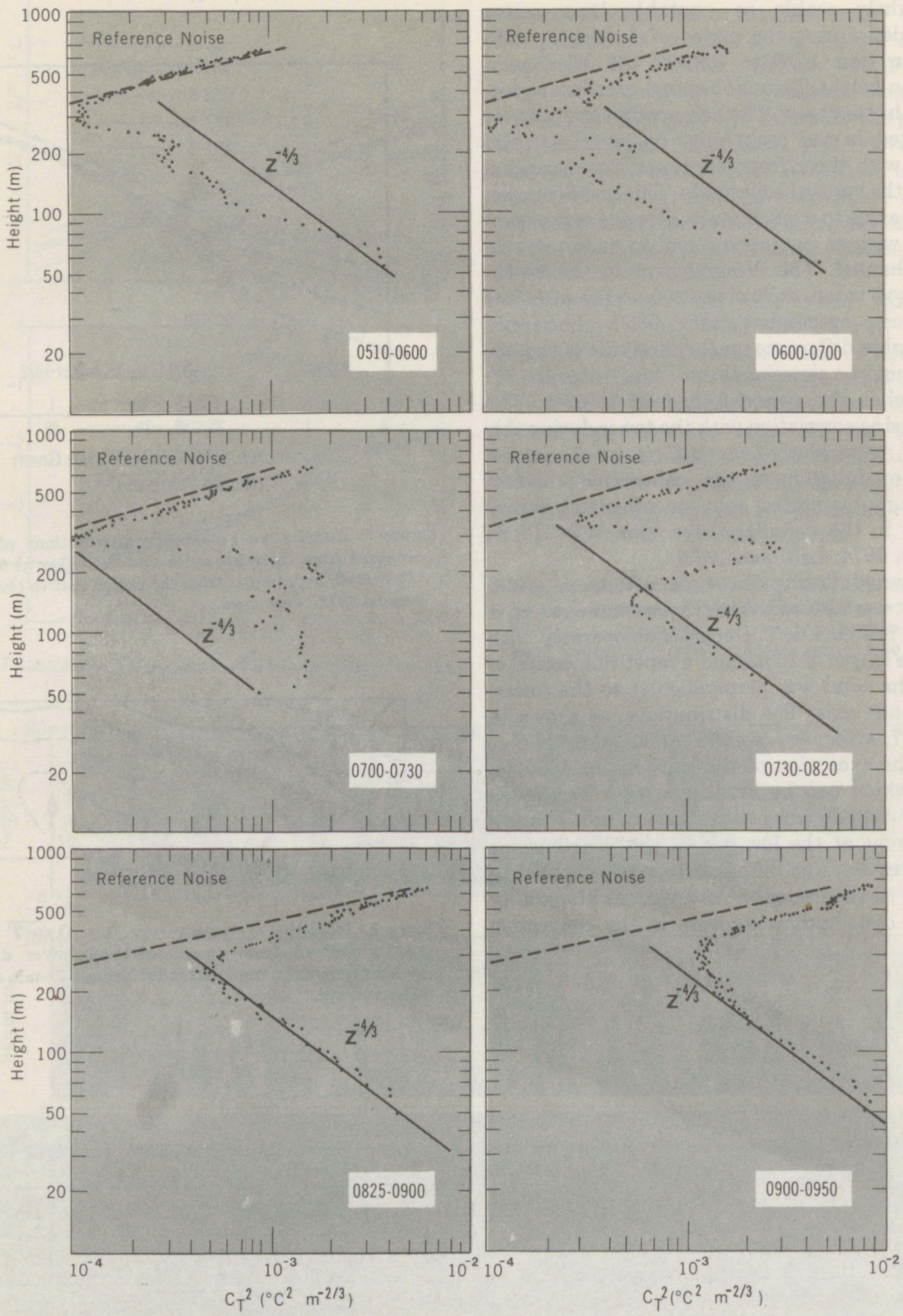

Figure 9. Profiles of C_T^2 to a height of 640 m from the vertical echosonde data are shown. Data were averaged in 2.7-m range gates over the time periods indicated. The theoretically predicted $Z^{-4/3}$ behavior of C_T^2 with height is shown, normalized to the values at 50 m. Reference noise levels are in terms of C_T^2.

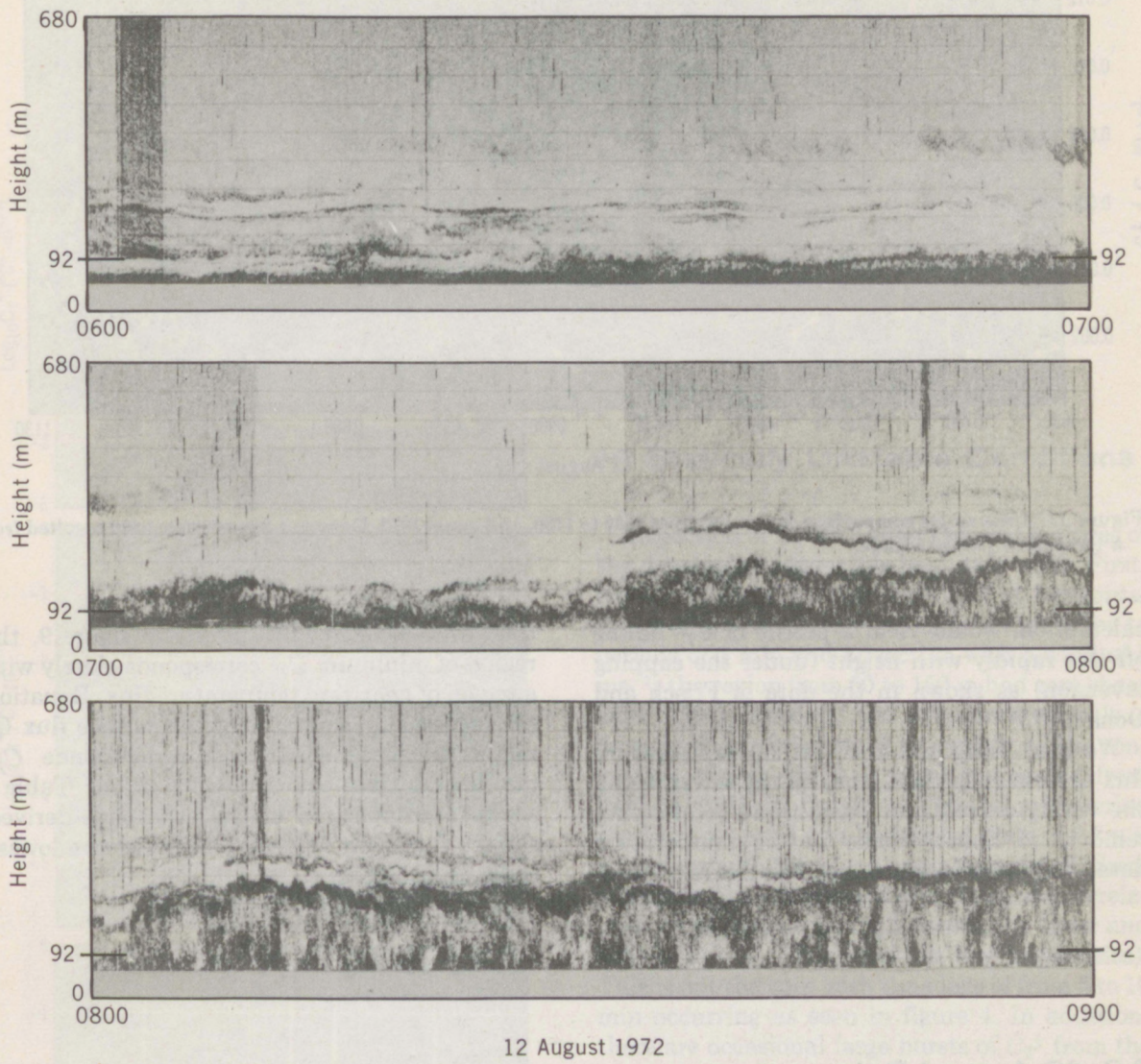

Figure 10. Echosonde facsimile record from 0600 to 0900, 12 August 1972.

case. Observation and simulation of such distributions are described by Lawrence et al. (1970).

Vertical profiles of C_T^2 were obtained by averaging the vertical echosonde data within each range gate to a maximum height of 650 m. Averaging times were chosen to correspond to periods of quasi-stationary inversion height. Such profiles are shown in figure 9 The predicted "$Z^{-4/3}$" dependence of C_T^2 (eq. 9) is shown, normalized to the values at the minimum reliable echosonde range of 50 m. Reference noise levels, posed in terms of C_T^2 and indicated in figure 9, were from data obtained during the 1-min break in the pulse transmission prior to each hour. As can be seen, the greatest contribution from the background noise level generally occurs above 400 to 500 m. The agreement of the predicted $Z^{-4/3}$ height-dependence of C_T^2 with the observed profiles in the period from 0825 to 0950 in figure 9 may be fortuitous since we have ignored, as an attenuation mechanism, the effective loss of energy from the beam which may result from nonreciprocal turbulent scattering. Such an "excess attenuation," if documented and included in the

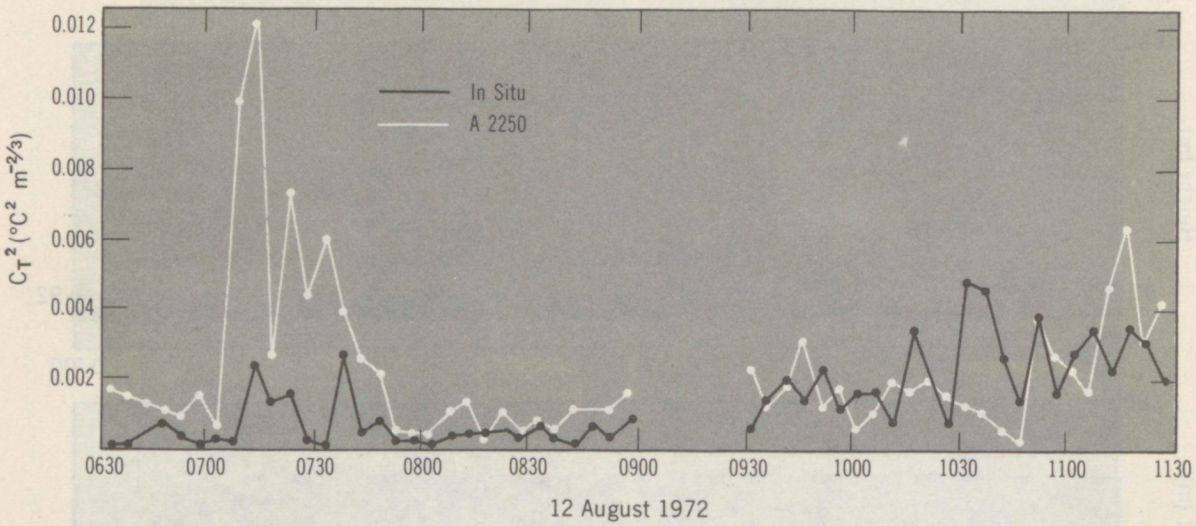

Figure 11. Time-series comparison for period from 0630 to 1130, 12 August 1972. Data gap from 0900 to 0930 resulted from a temporary power outage.

calculation, would yield a profile of C_T^2 falling off less rapidly with height (under the capping inversion) as shown in the data of Frisch and Ochs (1975).

We also computed the vertical temperature flux Q from each fixed level on the tower, using the eddy-correlation technique (following removal of linear trends in the temperature data). Isopleths of Q are shown in figure 8. From the "0730 to 0820 C_T^2" profile in figure 9, the region of minimum C_T^2 corresponds closely with a region of near-zero temperature flux. Equation (9) suggests that a value of the surface flux Q_0 might be obtained from the echosonde C_T^2 profile under free-convection conditions. Table 2 shows a comparison of the echosonde-derived surface flux with values obtained at the lowest tower level, 32 m.

3.2 12 August Data

The second case analyzed occurred on 12 August 1972. A portion of the facsimile record, shown in figure 10, reveals a temporal development on this day similar to that on the 15th. Because of an initially larger ground-based inversion, the development of the convective layer proceeds more slowly. The measurements in this case are not redundant, but were made with our principal operating frequency of 2250 Hz. The transition from statically stable to unstable conditions provides a calibration check between the two regimes. Figure 11 reveals the temporal development of C_T^2 at 92 m as obtained from each source. Figures 12a, b, and c provide the corresponding probability distributions in 1.5-hr blocks. The data gap from 0900 to 0930 was the result of a power failure.

As in the 15 August case, a larger echosonde-tower ratio occurs in the statically stable case (fig. 12a). This contrasts with the generally excellent agreement under the convectively unstable conditions which follow the inversion rise (fig. 12b). Following 1030, a longer term modulation of the convective activity is revealed in figure 11. The lack of correlation during this period ($\approx$1045) is similar to that found after 0900 on the 15th (fig. 4).

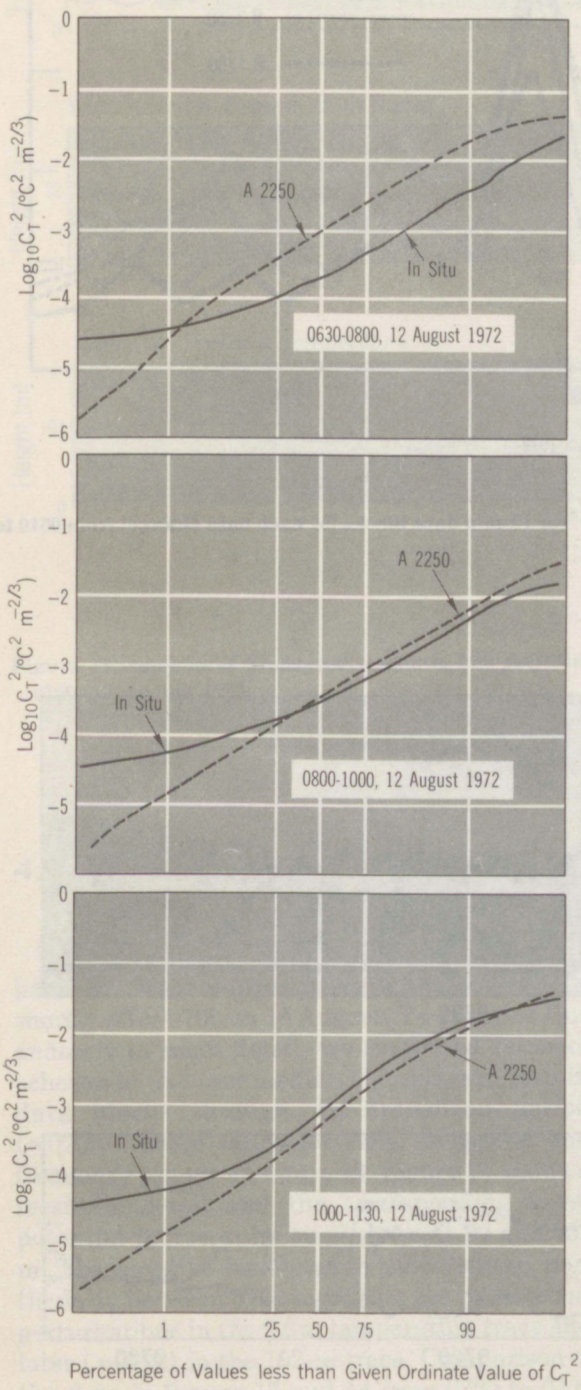

Figure 12. Cumulative probability distributions for 12 August 1972: (a) 0630 to 0800; (b) 0800 to 0900 and 0930 to 1000; and (c) 1000 to 1130. Echosonde pulse-repetition period was 4 s.

4. Discrepancies

4.1 Statically Unstable Conditions

Inspection of figure 3 shows several features of the developing convective boundary layer. First, regions of large C_T^2 are localized at horizontal scales of approximately 300 m (corresponding to periods of 1 min and advection with a wind of 5 ms^{-1}; the region from 50 to 150 m had zero shear after 0800). Second, the echosonde reveals a longer period variation of the height of the convection region which is most noticeable from 0925 to 0945 in figure 3. This 20-min period would correspond to a horizontal scale of 6 km if advection with the mean wind is assumed. Such a large length scale would suggest a good correlation at near-zero time lag between the tower and echosonde C_T^2 time series (at low frequencies). This is not the case with time lags of from 5 to 10 min occurring as seen in figure 4. In addition, there are occasional large bursts of C_T^2 from the tower that do not appear to correlate at all with those from the echosonde as from 1030 to 1045 in figure 11. Such "discrepancies" suggest the possible presence of slowly moving vortices, with the regions of large C_T^2 localized within fairly "narrow" updrafts. The correlation (or lack of it) between the tower and echosonde would depend on the motion and structure of such vortices.

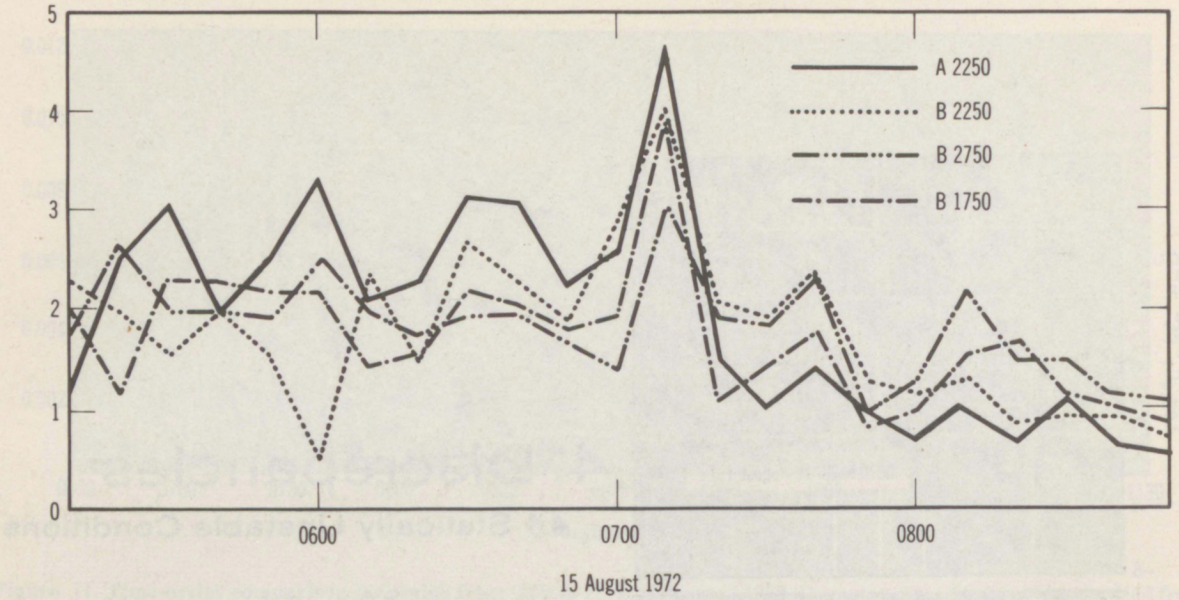

Figure 13. Ratios of echosonde median C_T^2 to tower median C_T^2 for 10-min data blocks for each data channel from 0510 to 0850, 15 August 1972.

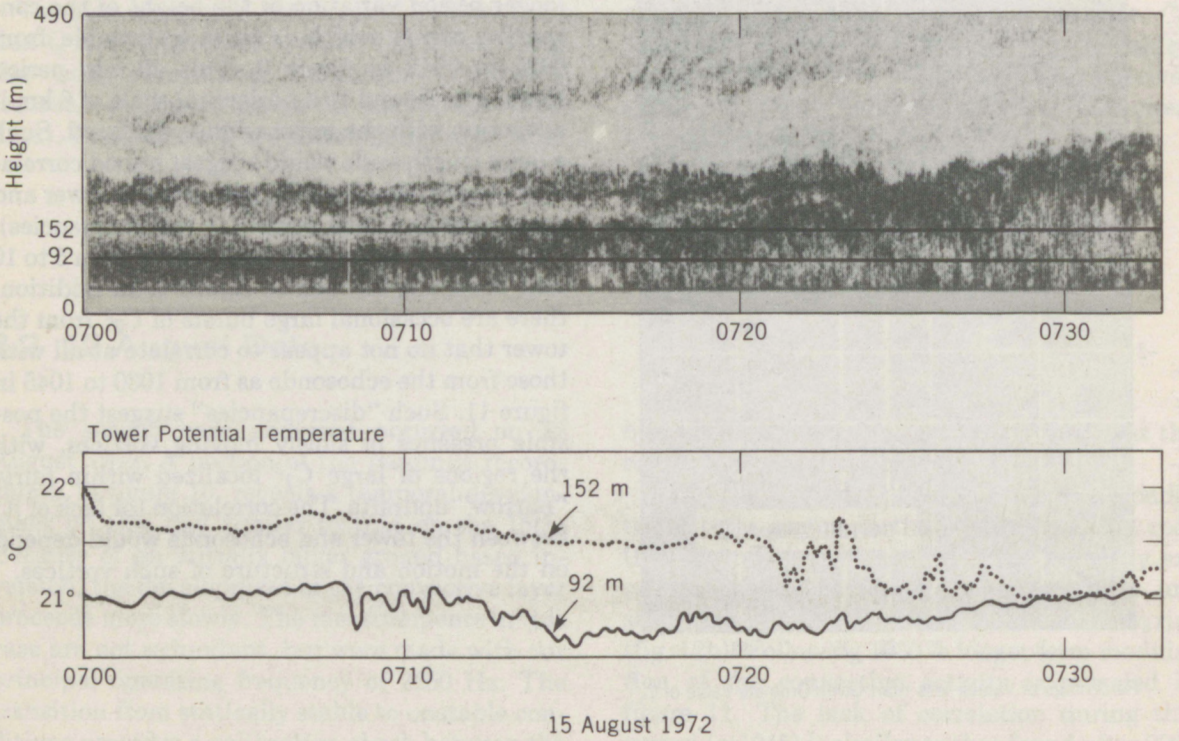

Figure 14. Facsimile detail with potential-temperature time series at 92 and 152 m for period of inversion rise from 0700 to 0735, 15 August 1972.

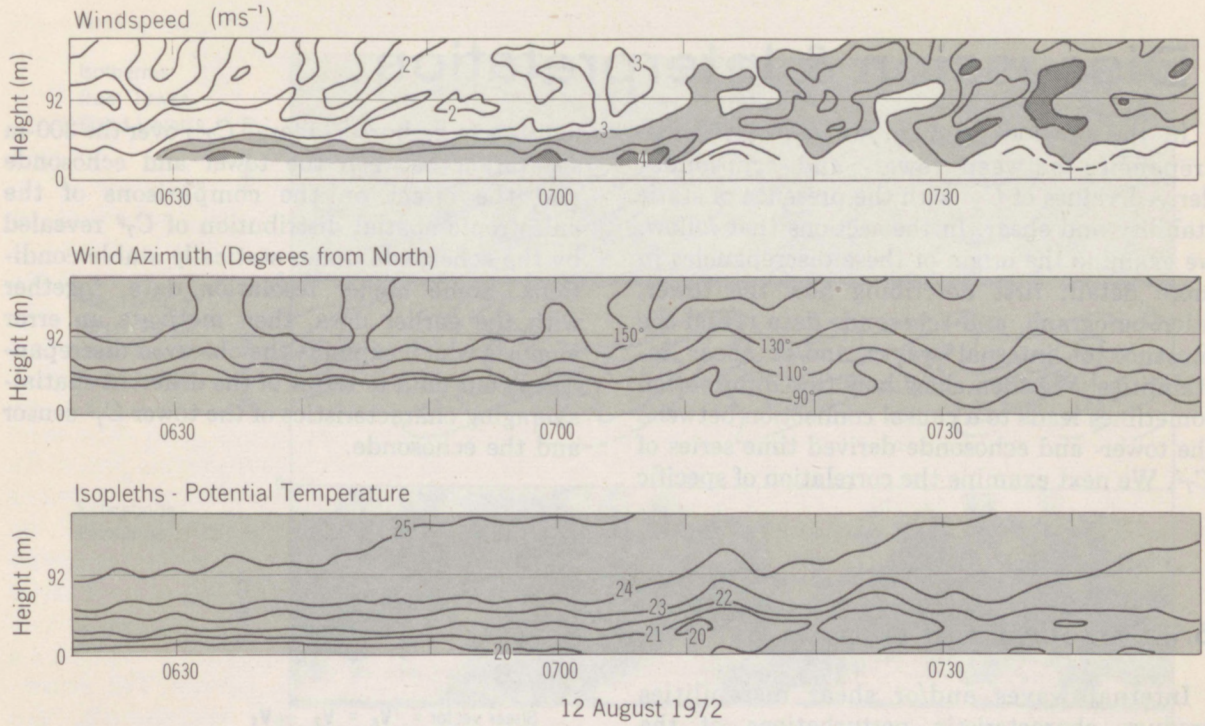

Figure 15.Isopleths of windspeed, azimuth, and potential temperature during the boundary layer transition from 0635 to 0750, 12 August 1972.

4.2 Statically Stable Conditions

Figure 4 shows a fairly marked disagreement between tower and echosonde values of C_T^2 shortly after 0700 on 15 August. To examine this anomaly in more detail, we computed ratios of echosonde-to-tower median C_T^2 values in 10-min data blocks through the transition period (≈0700). These ratios for each echosonde and frequency appear in figure 13. Figure 14 shows a facsimile detail and the corresponding tower potential-temperature time series at 92 and 152 m. The wavelike structures in the facsimile, particularly between 0708 and 0713, are reflected as perturbations in the 92-m temperature trace and later (≈0722) in the 152-m trace. Comparison of the data in figures 13 and 14 from 0700 to 0720 thus suggests a close connection between the presence of static stability and the observed anomaly. (This connection will be explored more fully in following sections.)

Figure 11 shows a marked discrepancy in the period from 0705 to 0735 on 12 August. Figure 15 shows the meteorological fields for the period from 0620 to 0750, contoured from the fixed-level tower data. These show the gradual warming of the layer near the ground prior to 0700 with little effect on the region above a few tens of meters. With the formation of a superadiabatic region near the ground after 0700, a longer period, higher amplitude, and more complicated oscillation of the boundary layer sets in. The lifting of the 3.5-ms^{-1} region and the relative cooling aloft bear a close similarity to features observed by Izumi (1964) in the breakup of a nocturnal jet. Figure 15 also shows a correspondence between the behavior of the azimuthal portion of the velocity field and the distribution of the potential temperature. Notable, also, is the enhancement of the directional shear and temperature gradients near the height of our comparisons during the period of maximum anomoly (cf., fig. 11).

5. Discussion & Interpretation

In the previous section, we associated discrepancies between tower- and echosonde-derived values of C_T^2 with the presence of static stability and shear. In the sections that follow, we examine the origin of these discrepancies in more detail; first describing how the tower, microbarograph, and echosonde data reveal the presence of internal waves and/or shear instabilities. We then show how this information sometimes leads to a causal connection between the tower- and echosonde-derived time series of C_T^2. We next examine the correlation of specific features (e.g., bursts of large C_T^2) over the 300-m separation between the tower and echosonde and the effect on the comparisons of the anisotropic spatial distribution of C_T^2 revealed by the echosonde under statically stable conditions. Some higher resolution data, together with the earlier data, then motivate an error analysis which explains the observed discrepancies in our data in terms of the different spatial-averaging characteristics of the tower C_T^2 sensor and the echosonde.

5.1 Correlation of Data

Internal waves and/or shear instabilities produce characteristic perturbations of the background temperature and velocity fields of the medium in which they propagate. The surface-level pressure variations, which they produce, allow a deduction of their horizontal phase speed and direction (through the use of microbarograph arrays as described, e.g., by Hooke et al., 1973). Such structures also may lead to the production of small-scale turbulence through local "wave"-induced increases in the shear (and tilting of the isopycnic surfaces) and the subsequent development of dynamic instability (e.g., Gossard et al., 1973). This turbulence acts on the background temperature gradients to produce temperature fluctuations at small scales which then serve as tracers for the echosonde. Restoring forces, which arise from the background static stability, and the transfer of kinetic energy to larger horizontal wavelengths (through the action of the background shear) also tend to localize the turbulence structure in relatively thin and patchy lamina. The echosonde graphically delineates the vertical structure and phase speed of such phenomena relative to the ground, thus motivating one's interpretation of both the tower and microbarograph data. The direct correlation of events at the tower and echosonde must,. however, be viewed with some caution because internal waves and their associated effect on the local dynamic stability of the flow can propagate rather arbitrarily, whereas the resulting shear instabilities (and turbulence) appear to advect

Shear vector = $\mathbf{V_S} = \mathbf{V_2} - \mathbf{V_1}$

Mean wind = $\mathbf{V_M} = \frac{\mathbf{V_1} + \mathbf{V_2}}{2}$

$\mathbf{V_1}$, $\mathbf{V_2}$ = Velocity at Levels 1 and 2, Respectively

$\mathbf{V_A}$ = Component of $\mathbf{V_M}$ Perpendicular to the Tower-Echosonde Axis

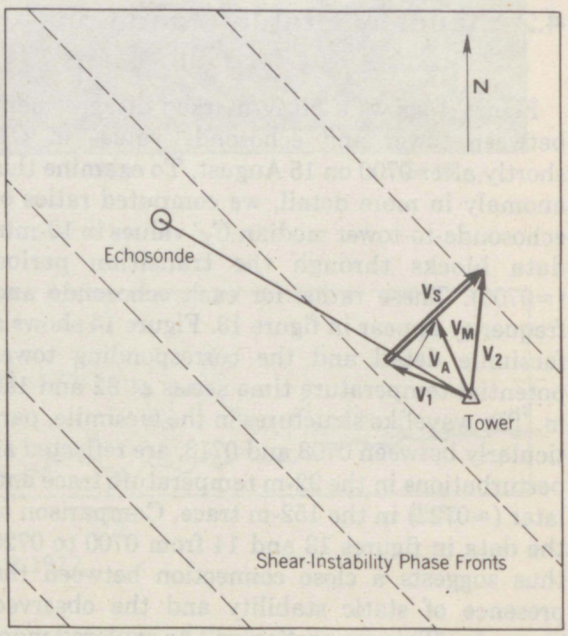

Figure 16. Illustration of shear-instability phase orientation in the flow with directional shear.

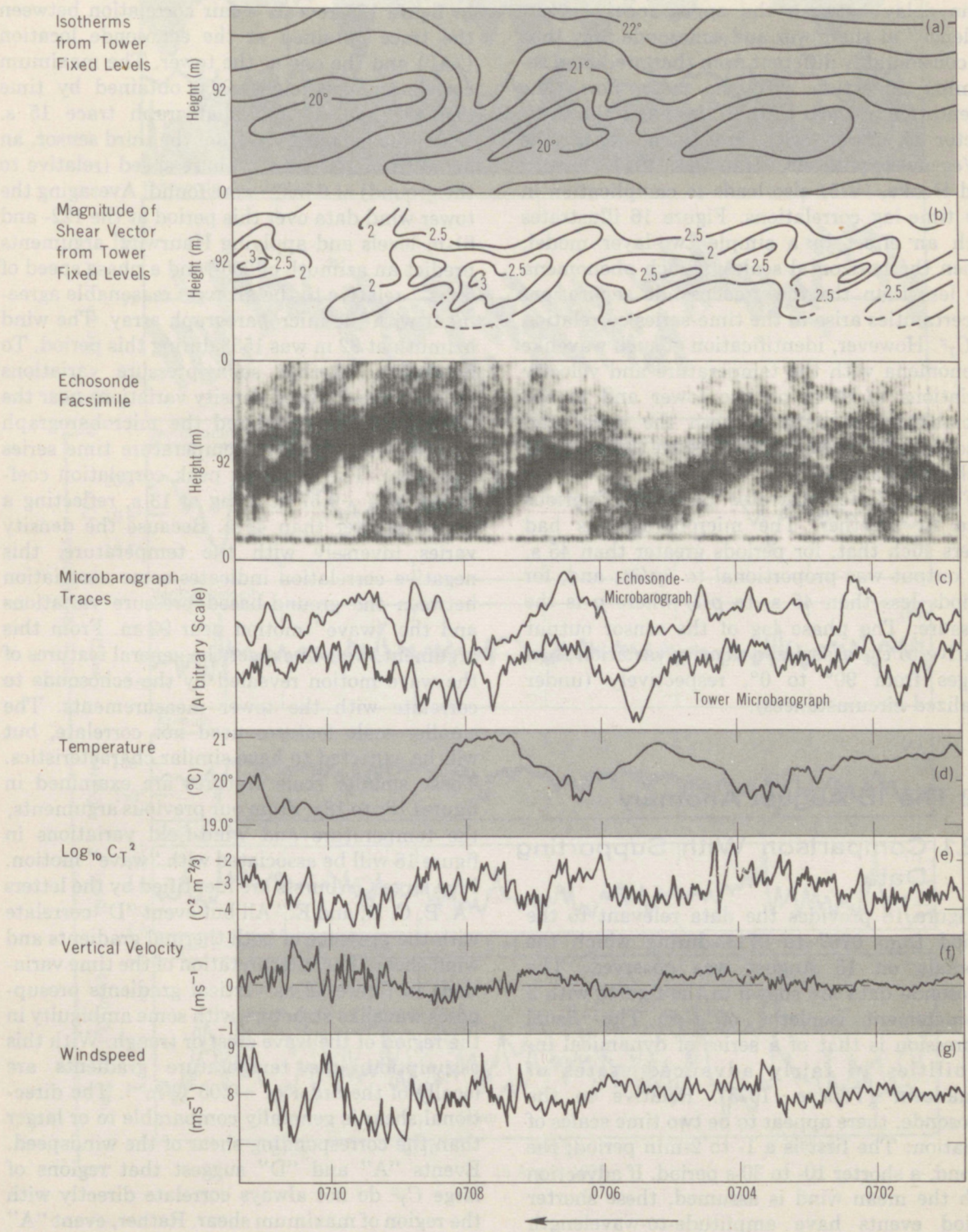

Figure 17. Echosonde facsimile record from 0702 to 0712, 16 August 1972: (a) isotherms obtained from fixed-level temperature data; (b) isopleths of shear vector magnitudes computed from 10-s averages at each fixed level ($= |\vec{v}_i - \vec{v}_{i+1}|$; "$i$" denotes the fixed levels taken at 30.48-m intervals); (c) microbarograph traces obtained at the echosonde and tower with zero time lag; (d) 92-m temperature trace showing a lag relative to the measurement of $\frac{\partial p}{\partial t}$ from the microbarograph; (e) tower C_T^2 trace showing bursts as the instabilities move past the tower; (f) vertical velocity trace (note the 90° phase lag relative to the temperature data); and (g) windspeed.

with the mean flow (Gossard et al., 1973). The time delay between the appearance of "turbulence" at the tower and echosonde may thus be considerably different from that predicted assuming advection with the mean flow. The orientation of shear instabilities along the shear vector in a flow with directional shear (the "Wegener hypothesis," Haurwitz, 1947; Gossard and Hooke, 1975) also leads to complication in the time-lag correlations. Figure 16 illustrates such an effect in a simple two-layer model. When the horizontal scales of such phenomena are less than the tower-echosonde separation, uncertainties arise in the time-series correlation of C_T^2. However, identification of such wavelike phenomena with the temperature and velocity variations at 92-m on the tower and in the microbarograph data at both the tower and echosonde locations helps to resolve the source of such uncertainties.

Figure 17 demonstrates how these various data fit together. The microbarographs had filters such that, for periods greater than 45 s, the output was proportional to $\partial p/\partial t$; and, for periods less than 45 s, to $p(t)$ where p is the pressure. The phase lag of the sensor output relative to the associated density variation then ranges from 90° to 0°, respectively (under idealized circumstances).

5.2 The 15 August Anomaly

5.2.1 Comparison With Supporting Data

Figure 18 provides the data relevant to the period from 0707 to 0714 during which the anomaly on 15 August was observed. The echosonde data are shown in the figures with 3 dB-increment isopleths of C_T^2. The visual impression is that of a series of dynamical instabilities in fairly advanced states of breakdown (Thorpe, 1973). Relative to the echosonde, there appear to be two time scales of variation: The first is a 1- to 2-min period; the second, a shorter 10- to 30-s period. If advection with the mean wind is assumed, these shorter period events have amplitude-to-wavelength ratios ranging from 1:4 to 1:7. For shear instability events, the slope in the facsimile reveals the sign of the shear of the windspeed. We also note that the echosonde does not distinguish *a priori* between descending layers and advecting tilted layers.

An inspection of the microbarograph records in figure 18a reveals a fair correlation between the trace obtained at the echosonde location ("A") and the one at the tower. The maximum correlation coefficient=0.60 obtained by time lagging the "A" microbarograph trace 15 s. Using the lag observed from the third sensor, an azimuth of 190° and a phase speed (relative to the ground) of 6 ms^{-1} were found. Averaging the tower wind data over this period at the 122- and 61-m levels and applying Haurwitz' arguments predict an azimuth of 205° and a phase speed of 5 ms^{-1} relative to the array in reasonable agreement with the microbarograph array. The wind azimuth at 92 m was 155° during this period. To determine whether such pressure variations reflect wave-induced density variations near the 92-m level, we correlated the microbarograph output with the 92-m temperature time series (fig. 18a). The resulting peak correlation coefficient was −0.57 at a lag of 13 s, reflecting a period greater than 45 s. Because the density varies inversely with the temperature, this negative correlation indicates some association between the ground-based pressure variations and the "wave" motion near 92 m. From this argument, we will expect the general features of the wave motion revealed by the echosonde to correlate with the tower measurements. The smaller scale features need not correlate, but will be expected to have similar characteristics. These smaller scale features are examined in figures 18c to 18g. From our previous arguments, the temperature and wind-field variations in figure 18 will be associated with "wave" motion. Five large C_T^2 bursts are identified by the letters "A, B, C, D, and E." All but event "D" correlate with the presence of both thermal gradients and wind shear. The interpretation of the time variations in figure 18 as vertical gradients presupposes wavelike structure with some ambiguity in the region of the wave crest or trough. With this assumption, the temperature gradients are locally of the order of +0.05°C m^{-1}. The directional shear is generally comparable to or larger than the corresponding shear of the windspeed. Events "A" and "D" suggest that regions of large C_T^2 do not always correlate directly with the region of maximum shear. Rather, event "A" suggests, as does figure 17, that larger thermal gradients bound the region of intense small-scale turbulence (as revealed in the C_T^2 measurements). This effect would presumably arise from the smoothing action of the eddy-fragmentation process on the gradients in the

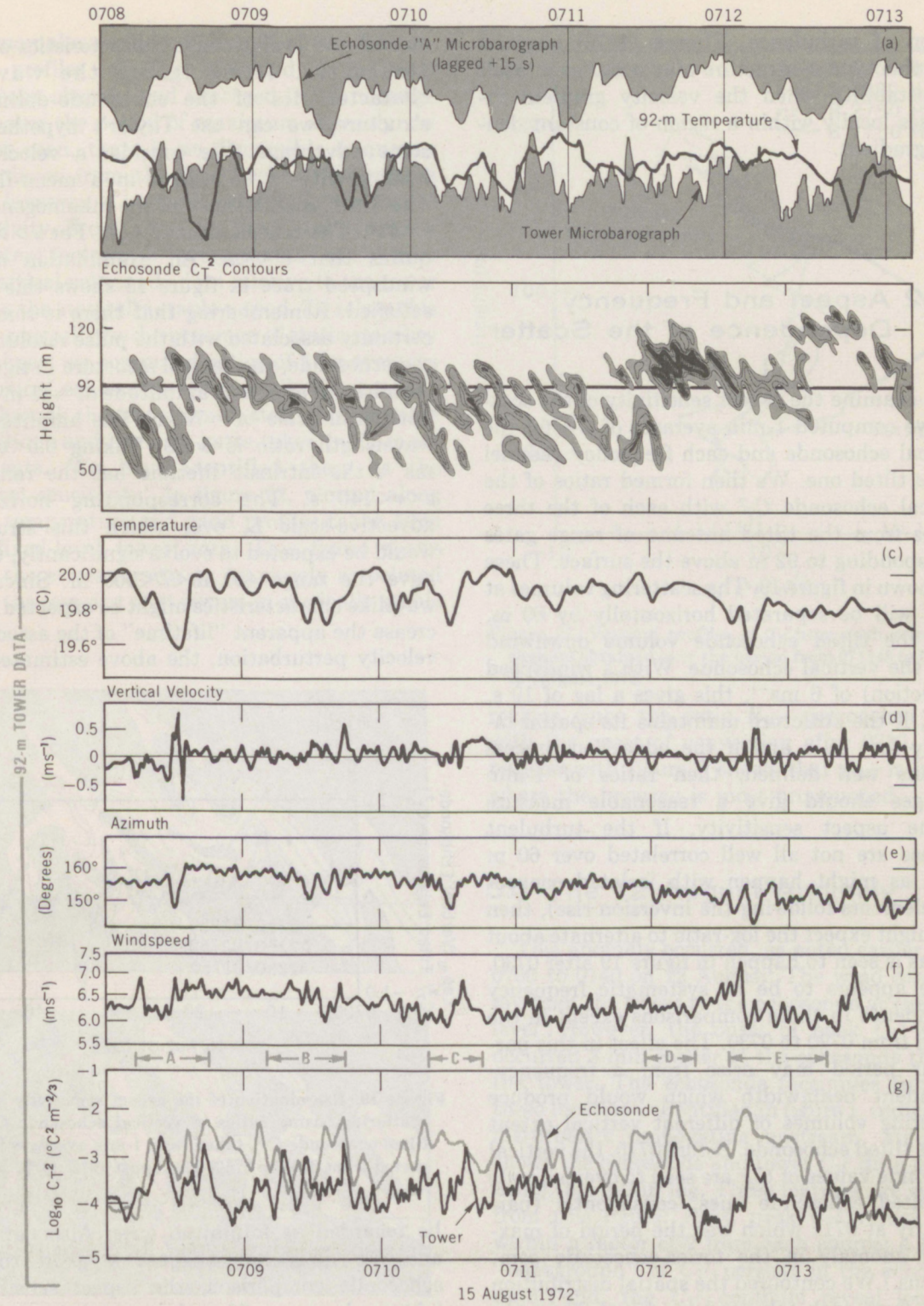

Figure 18. Detailed echosonde contours (3-dB increment in C_T^2 isopleths; minimum equals 0.00125°C $m^{-2/3}$) for period from 0708 to 0713, 15 August 1972: (a) microbarograph at tower base compared with pressure recording at echosonde "A" lagged 15 s; and compared with temperature variation at 92-m level (microbarograph output is proportional to $p(t)$ and $\frac{\partial p(t)}{\partial t}$, depending on the period of the motion); (c) 92-m tower time series of temperature; (d) 92-m tower time series of vertical velocity; (e) 92-m tower time series of azimuth from north; (f) 92-m tower time series of windspeed; and (g) 92-m tower time series of *in situ* C_T^2.

region of turbulence. Thorpe (1973) suggests that this type of structure may occur as a result of instability when the velocity gradient increases locally within a region of constant density gradient.

5.2.2 Aspect and Frequency Dependence of the Scatter

To examine the aspect sensitivity of the scatter, we computed 1-min averages of C_T^2 for the vertical echosonde and each frequency channel of the tilted one. We then formed ratios of the vertical echosonde C_T^2 with each of the three values from the tilted antenna at range gates corresponding to 92 m above the surface. These are shown in figure 19. The scattering volumes at 92 m will be separated horizontally by 60 m, with the tilted echosonde volume downwind from the vertical echosonde. With a windspeed (advection) of 6 ms^{-1}, this gives a lag of 10 s. Thus, if the structure maintains its spatial integrity for 10 s and if the advection process remains well defined, then ratios of 1-min averages should give a reasonable measure of the aspect sensitivity. If the turbulent patches are not all well correlated over 60 m (such as might happen with isolated convective elements following the inversion rise), then one might expect the log-ratio to alternate about zero as is seen to happen in figure 19 after 0730. There appears to be no systematic frequency dependence in these comparisons except in the period from 0720 to 0730. The effect in this particular period may arise from a frequency-dependent beamwidth which would produce scattering volumes of different vertical extent for the tilted echosonde. Before 0715, the vertical echosonde values of C_T^2 are seen to overestimate the tilted echosonde ones, consistently (particularly at 0712 which was the period of maximum anomaly in the tower-echosonde comparisons.) We contoured the spatial distribution of C_T^2 from each echosonde in figure 20 for the period from 071148 to 071248. Because the horizontal motion of a patch through the tilted beam will produce an apparent vertical motion, some ambiguity should be expected in comparing the spatial distributions in this figure. However, the apparent geometrical distortion, revealed in figure 20, suggests a brief look at the spatial and evolutionary characteristics of such structures. If we ignore the wavelike characteristics of the echosonde-delineated structure, we can use Taylor's hypothesis to some advantage. We consider a velocity inhomogeneity v' of scale l in a mean-flow u. The "intrinsic lifetime" of the inhomogeneity is $\tau = l/v'$. The transit-time $T = l/u$. For $\tau >> T$ requires that $v' << u$. An examination of the windspeed trace in figure 18 shows this to be satisfied. Remembering that there is some uncertainty associated with the pulse resolution of the echosonde, the central structure in figure 20 then has an apparent amplitude of ≈11 m and a horizontal scale of ≈70 m. The amplitude-to-wavelength ratio is ≈1:6. Taking $0.5 < v' < 1.0$ ms^{-1}, the intrinsic lifetime has the range 70 $s < \tau < 140$ s. The corresponding horizontal advective-scale L, over which this structure would be expected to evolve significantly, would have the range 450 $m < L < 900$ m. Since any wavelike characteristics might be expected to increase the apparent "lifetime" of the associated velocity perturbation, the above estimates will

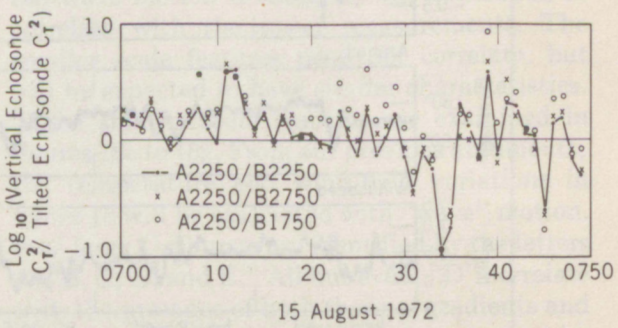

Figure 19. Examination of the aspect sensitivity of the scattering, using ratios of vertical echosonde C_T^2 to tilted echosonde C_T^2, taken from 1-min averages in the period from 0700 to 0750, 15 August 1972, at 92 m.

be regarded as minimum ones. Although this analysis does not suggest a good tower-echosonde comparison, the aspect sensitivity (obtained over a 60-m horizontal separation) would be expected to have some validity. (Any internal inhomogeneities in such a structure could lead to aliasing difficulties with respect to the echosonde's discrete sampling rate: This is a possible explanation for the large apparent anomaly at 071240 in fig. 20.) We also examined the frequency dependence of the scatter from

this anomalous region. Figure 21 shows the vertical profiles of C_T^2 obtained from each frequency channel and averaged in 2.7-m range gates over the period of maximum anomaly. As can be seen, there is no discernible frequency dependence from the tilted echosonde returns with, however, a marked anomaly in the aspect sensitivity. From figure 13, there also appears a persistent factor-of-2 "overestimate" of C_T^2 from the vertical echosonde data relative to the tower during the statically stable period. To relate this more generally to the presence of static stability and shear, we computed ratios of 1-hr averages of vertical echosonde C_T^2 and tilted echosonde C_T^2 through the transition to statically unstable conditions and at range gates taken in 25-m increments. We have identified these as the "aspect sensitivity" in figure 22, plotted along with temperature and wind profiles taken from the fixed-level tower data. This figure shows that the errors appear to be closely associated with the layering that occurs in statically stable

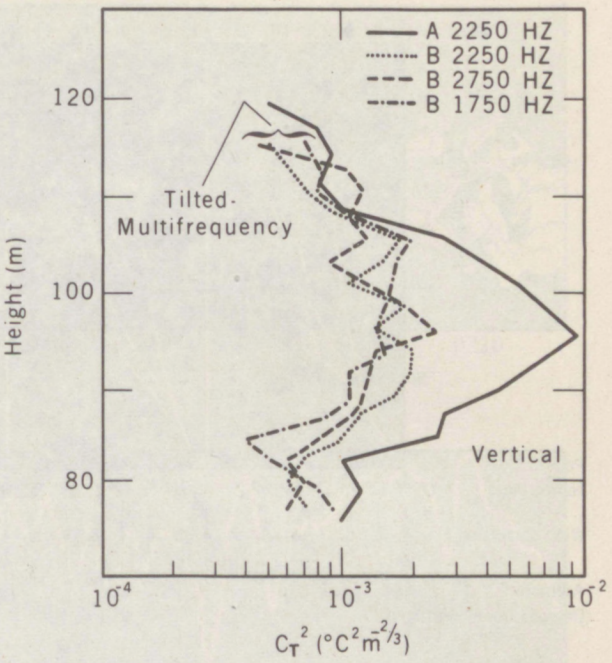

Figure 21. Vertical profiles of C_T^2 from each echosonde channel obtained over the period from 071148 to 071248, 15 August 1972.

regions since the ratio R_{VT} approaches unity with the onset of convection after 0710. Comparison with figure 3 shows that R_{VT} is largest where the layering is most pronounced.

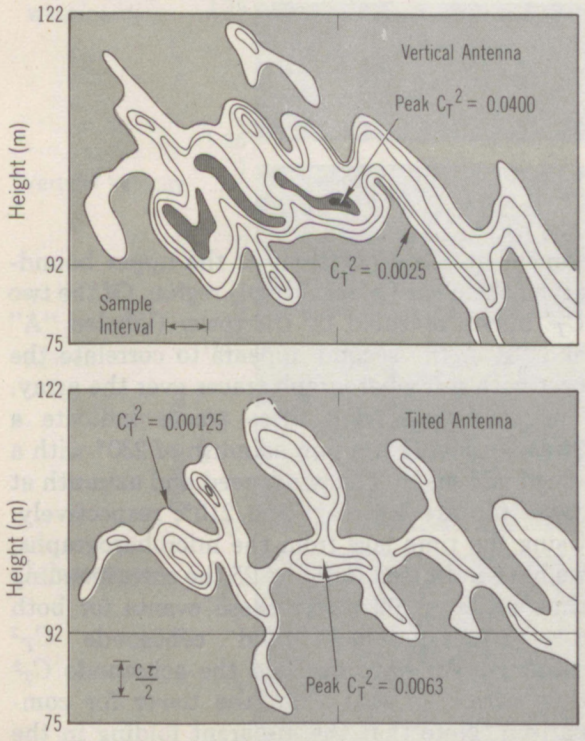

Figure 20. Isopleths of C_T^2 from the vertical echosonde at 2250 Hz (top) and the tilted echosonde at 2750 Hz (bottom) for the region of maximum return from 071148 to 071248, 15 August 1972. The tilted echosonde data were corrected for distortion resulting from height-dependent time lags, using the tower mean wind.

5.3 The 12 August Anomaly

This anomaly occurred, as noted earlier, from 0700 to 0740 on 12 August. The wind direction lay from the tower to the echosonde at the 92-m level. However, the onset of peak C_T^2 values occurred 3 min earlier at the echosonde than at the tower. The echosonde facsimiles from the three locations, identified in figure 1, indicated a disturbance propagating upstream. Figure 23 shows the echosonde and tower C_T^2 data plotted using this 3-min lag. Three features are evident from this figure: First, peak C_T^2 values agree within a factor of 2 from each source; a higher "background" of C_T^2 persists in the echosonde data; and, the C_T^2 contours reveal localized intense "turbulent" patches distributed along generally horizontal sheets.

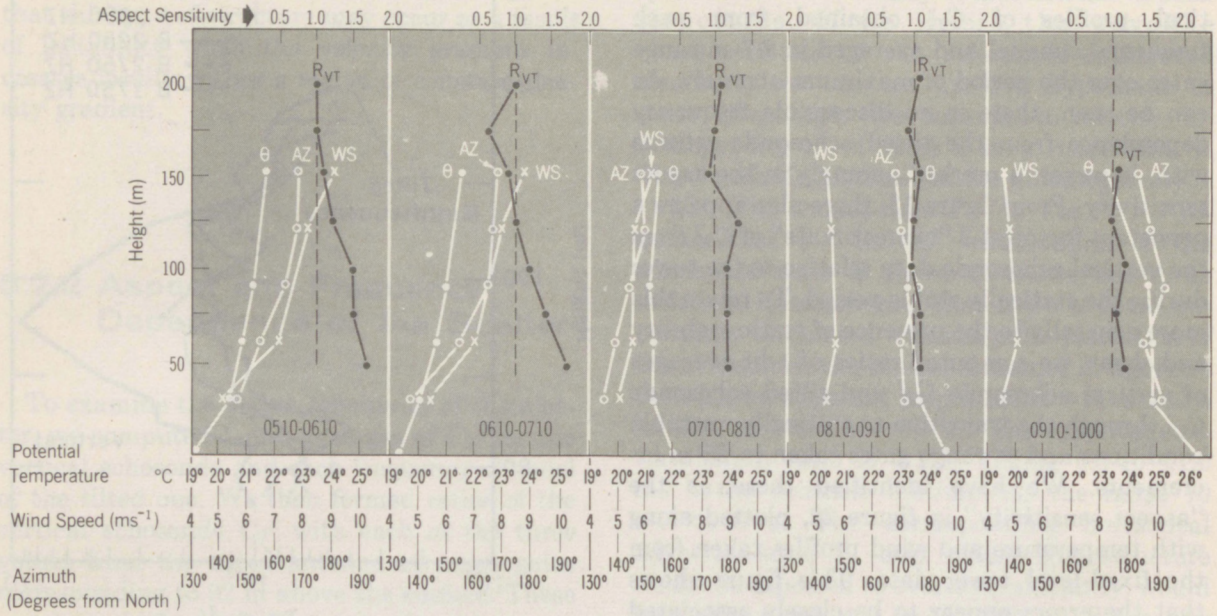

Figure 22. Hourly averaged profiles from the tower fixed levels of windspeed, azimuth, and potential temperature for 15 August 1972 case, with the corresponding ratio R_{VT}, of vertical echosonde C_T^2 to tilted echosonde C_T^2 at 2250 Hz.

5.4 Special Cases

We examined several additional cases where the tower and echosonde-derived values of C_T^2 were in agreement and which revealed specific features of the spatial distribution of C_T^2 under statically stable conditions. The first case was obtained with a particularly short pulse-length of 6 ms and under fairly well-defined inversion conditions. The facsimile record and isopleths of potential temperature from the tower appear in figure 24. We examined a single event that showed a strong correlation between the tower and echosonde obtained during the period from 0110 to 0112. The tower measurements and microbarograph-array records are shown in figure 25 along with the computer-expanded contours of C_T^2 from the echosonde. We used here a 2-s repetition period to delineate the structure horizontally. Our echosonde analog data were sampled routinely at 2 ms and averaged to 16 ms, yielding a vertical spatial resolution of 2.7 m. This compares with the 2-m spatial scale of the 6-ms pulse. The microbarograph traces appear to reflect somewhat the oscillations of the upper boundary of the clear (≈isothermal) region. Of the two C_T^2 bursts revealed by the tower (labeled "A" and "B"), the second appears to correlate the best with microbarograph traces over the array. The time lags from these traces indicate a "wave" moving from an azimuth of 230° with a speed of 5 ms^{-1}. The windspeed and azimuth at tower top are 4.6 ms^{-1} and 210°, respectively. Using the time lags from the microbarographs, we have indicated in figure 25 the corresponding time series at 92 m for these events for both tower measurements and echosonde C_T^2 contours. We have overlaid the echosonde C_T^2 time series on that from the tower for comparison. Note that the apparent folding in the contours is indicated in the vertical velocity trace. The thermistor time constant was too slow to reveal a similar variation in the temperature. Case "A" which does not show as clearly in the C_T^2 comparisons also is not clearly reflected in the microbarograph traces.

A case that shows patches localized both

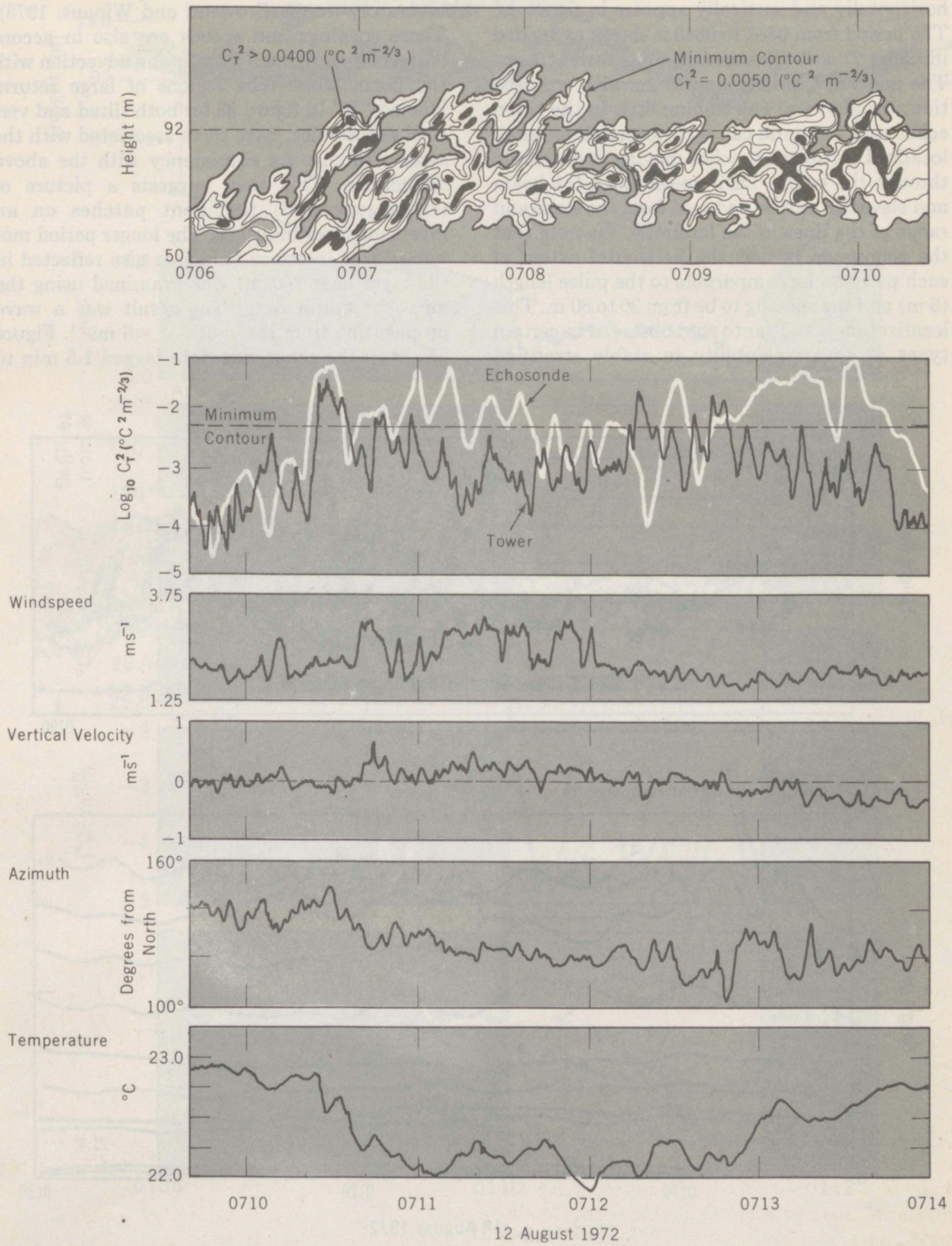

Figure 23. Echosonde-derived isopleths of C_T^2 (for a period of maximum anomaly) compared with fixed-level tower data for the period from 0710 to 0714, 12 August 1972.

horizontally and vertically appears in figure 26. The period from 0643 to 0648 is shown expanded in figure 27 with the corresponding tower traces. The pulse length here was 20 ms with a repetition period of 4 s. The sloping lines in the tilted echosonde facsimile can be interpreted as small localized turbulent patches moving horizontally through the beam. Their speed along the beam and elevation can be deduced from the slope and range of the lines in the facsimile. We note that the echosonde reveals the horizontal extent of each patch to be comparable to the pulse length (6 m) and the spacing to be from 30 to 80 m. This localization is similar to that observed in certain types of shear instability in stably stratified laboratory fluids (Browand and Winant, 1973). These spacings and speeds are also in accord with those in figure 27, assuming advection with the mean wind. The regions of large return, labeled "B" in figure 26 for both tilted and vertical echosondes, have to be associated with the same structure for consistency with the above deductions. This then suggests a picture of (shear-generated) turbulent patches on an inversion-shear interface. The longer period motion of this interface (which is also reflected in the layer near 200 m) was examined using the microbarograph data. The result was a wave propagating from the south at ≈ 6 ms^{-1}. Figure 27 shows the echosonde data lagged 1.5 min to

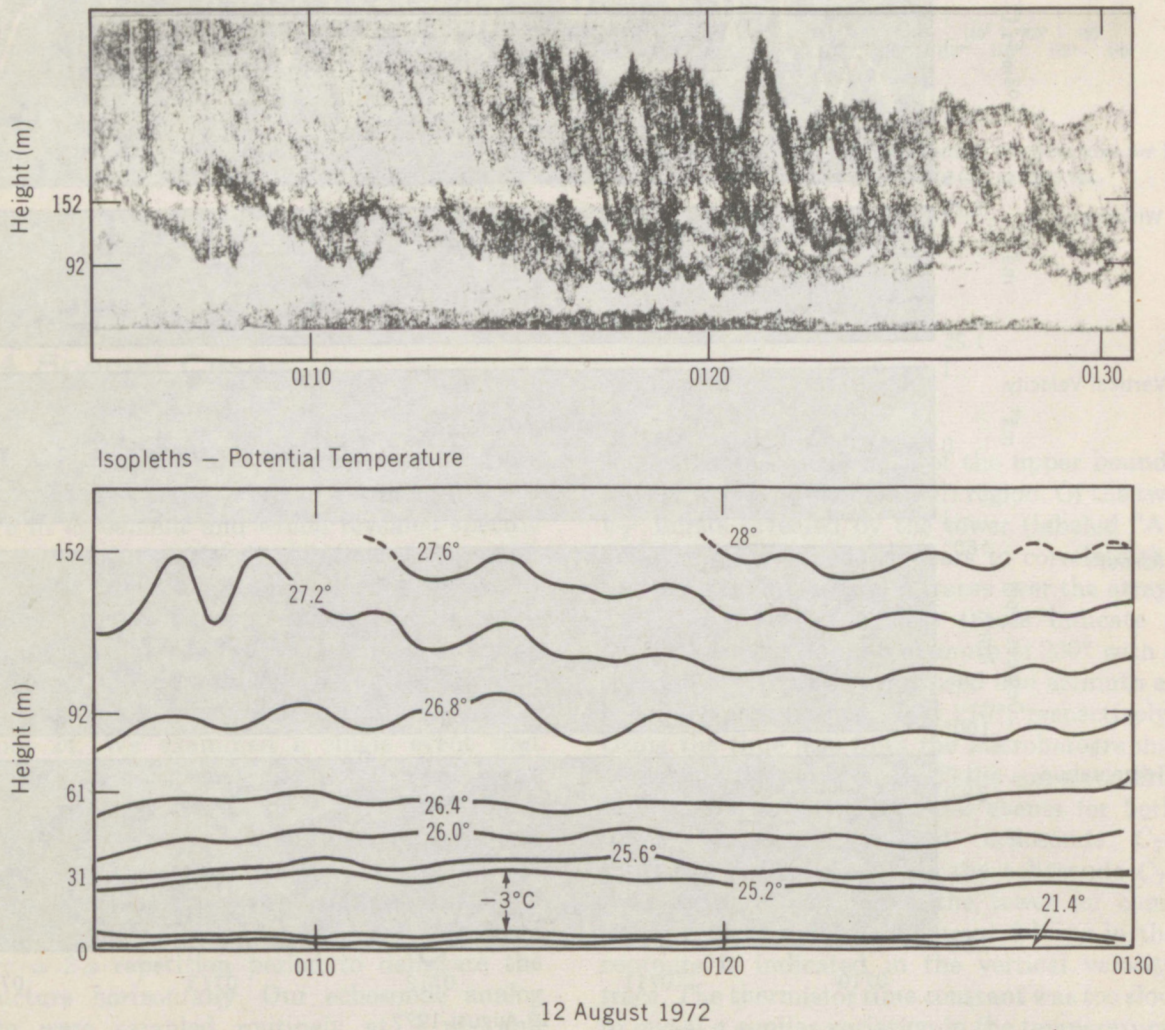

Figure 24. Facsimile detail for period from 0104 to 0132, 12 August 1972, obtained with a pulse repetition period of 2 s and a pulse length of 6 ms and compared with potential temperature contours that were obtained using fixed-level tower data.

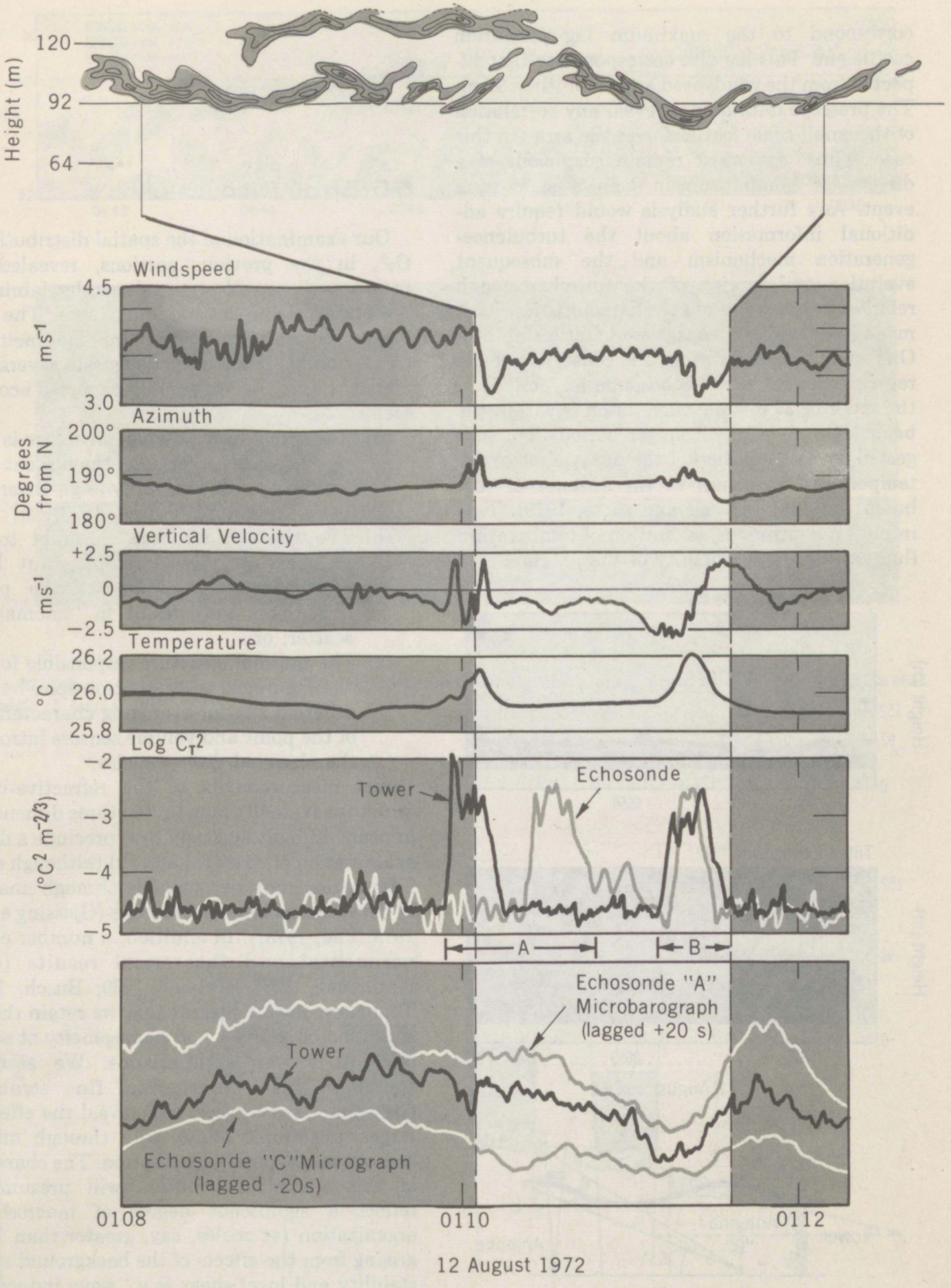

Figure 25. Examination of an isolated scattering layer near 92 m, using the echosonde-derived isopleths of C_T^2, microbarograph data, and the 92-m fixed-level tower data from 0108 to 0112, 12 August 1972.

correspond to the maximum lag-correlation coefficient. This lag also corresponds to that expected from the windspeed and azimuth at 92 m. The pressure data do not reveal any correlation of the small-scale features over the array in this case. Thus, one must remain suspicious of a direct C_T^2 comparison in such a short-term event. Any further analysis would require additional information about the turbulence-generation mechanism and the subsequent evolution and motion of the turbulent patch relative to the wave phase characteristics, local mean flow, and the background static stability. One should note, however, the constancy of the return from the tilted echosonde for periods of the order of 30 s while each patch is within the beam. This is a much longer period than suggested by a calculation of the decay time of the temperature spectrum in the absence of turbulent mixing (Metcalf and Atlas, 1973). This implies a continuous generation of temperature fluctuations in the vicinity of the patch.

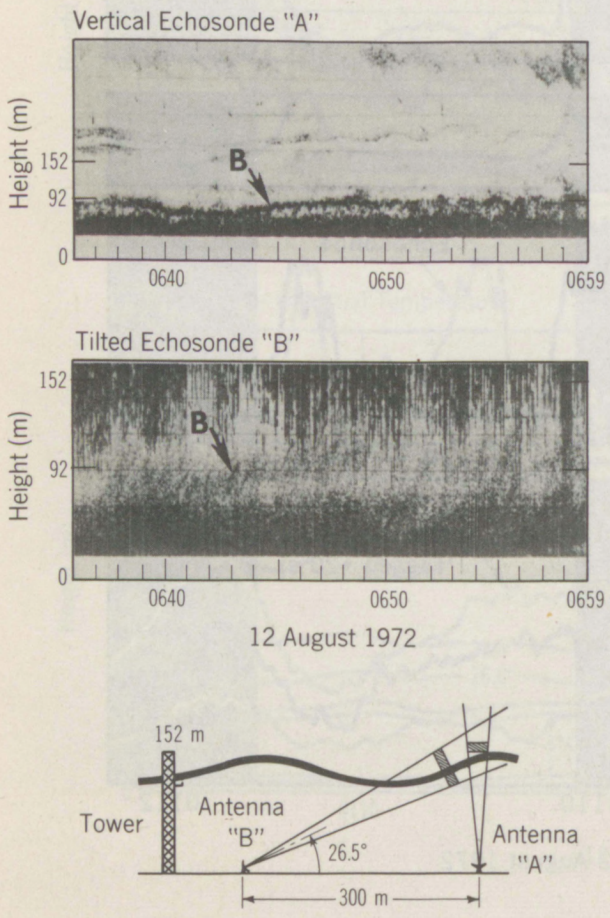

Figure 26. Examination of "turbulent" patches on an isolated layer, utilizing vertical and tilted echosondes from 0636 to 0659, 12 August 1972.

5.5 Error Discussion

Our examination of the spatial distribution of C_T^2, in the previous sections, revealed the presence of quasi-horizontal patchy lamina in the stably stratified boundary layer. The high degree of anisotropy and inhomogeneity in these spatial distributions suggests several explanations for the larger-than-expected acoustic scatter:

(a) The small-scale thermal structure is non-turbulent and, therefore, the present scatter theory does not apply (e.g., Ottersten, 1970; Metcalf and Atlas, 1973); or,

(b) The thermal structure internal to the patches may be isotropic, but large temperature gradients at the patch boundaries may result in "anomalous" scatter; or,

(c) The thermal structure responsible for the observed echo is locally isotropic, but the different spatial-averaging characteristics of the point and volume sensors introduce the observed discrepancies.

Direct measurements of the refractive-index structure at small scales and in three dimensions appears difficult and may thus preclude a direct examination of cases (a) and (b) (although some information may be available through analysis of data from point-sensor arrays (Gjessing et al., 1973; Pao, 1973)). In addition, a number of experimental and theoretical results (e.g., Kraichnan, 1966; Kaimal, 1969; Busch, 1973; Tennekes, 1973b) suggest that we retain the assumption of isotropy and homogeneity at scales relevant to our comparisons. We assume, therefore, that the thermal fine structure (parameterized by C_T^2) will reveal the effect of larger anisotropic eddys only through an inhomogeneous spatial distribution. The character of this spatial distribution will presumably reflect a significant degree of macroscopic organization (at scales, say, greater than 1 m) arising from the effects of the background static stability and local shear (e.g., wave induced).

To evaluate the magnitude of the sampling errors under such conditions, we examined the patch geometry shown in figure 28. The shaded area represents the apparent echo for a pulse

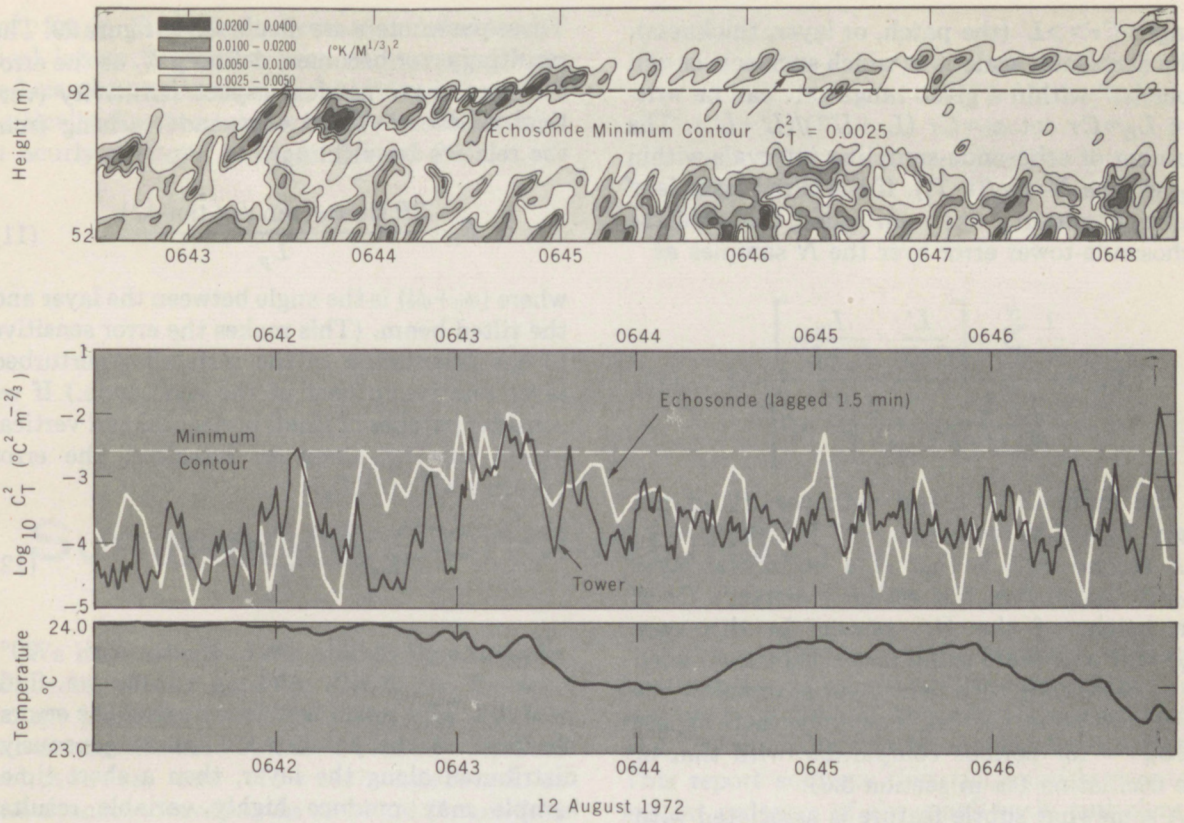

Figure 27. Echosonde-derived isopleths of C_T^2 compared with *in situ* C_T^2 and temperature at 92 m for the period from 0641 to 0647, 12 August 1972.

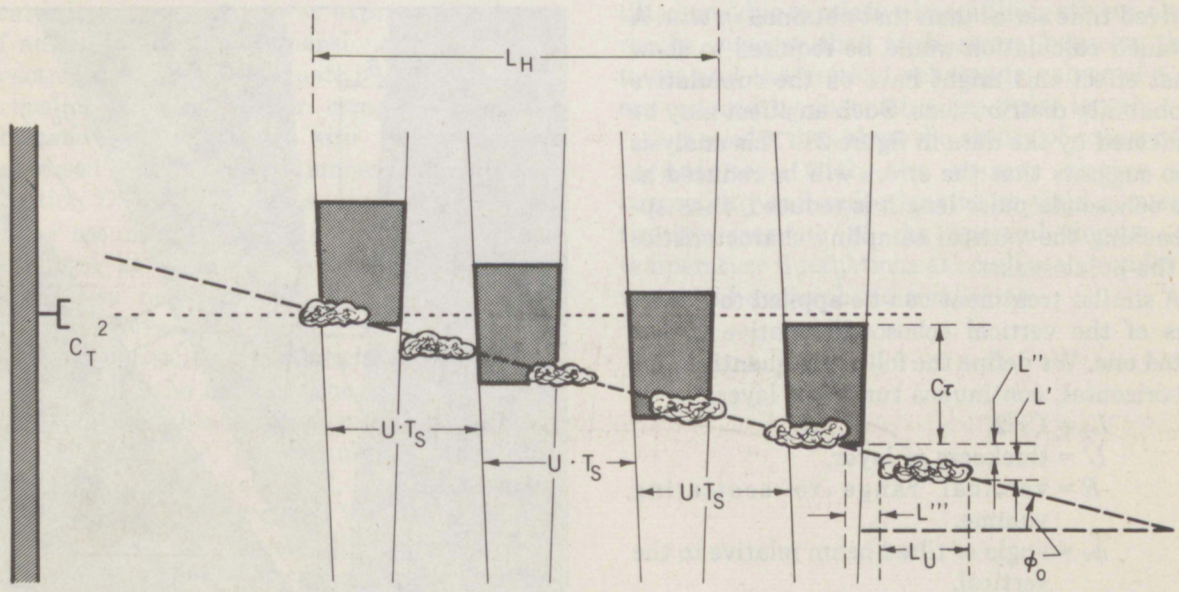

Figure 28. Schematic diagram for computation of the relative echosonde-tower error. The shaded area represents the observed echo within a fixed range gate for a pulse length $c\tau$.

length $C\tau >> L'$ (the patch, or layer, thickness). The horizontal scale over which such echoes will "persist" within a given range gate can be written $L_H = C\tau \cot \phi_0 = C\tau\ (L_u + L''')/(L' + L'')$. The number of echosonde-sampling intervals within L_H will be $N = L_H/(u \cdot T_s)$. If the tilted layer is of infinite extent, one can pose the relative echosonde-tower error over the N samples as

$$E_R = \frac{\frac{1}{N}\sum_{i=1}^{N}\left[\frac{L'}{C\tau/2}\cdot\frac{L_u}{L_u+L'''}\right]}{\frac{1}{N}\left[\frac{L'}{L'+L''}\cdot\frac{L_u}{u\cdot T_s}+0\right]} = 2 \qquad (10)$$

in the limit $C\tau >> L'$ and with the tilt of the "layer" given by $\cot \phi_0 = (L_u + L''')/(L' + L'')$.

A second case is that of a horizontal layer ($\phi_0 = 0$) just below, but within a distance $C\tau$ of the height of the C_T^2 sensor. In this case $E_R \to \infty$. For a more complicated geometry, such as an oscillating turbulent layer at or below our 92-m comparison level, one may then expect $2 < E_R < \infty$ for periods comparable with that of the oscillation (as in section 5.3).

A somewhat subtle feature is associated with our assumption that $L' << C\tau$. This assumption was made to avoid the problem of including the spatial convolution of the pulse with some assumed spatial distribution of C_T^2. If this possibility is included, one might expect a higher "background" of C_T^2 in the echosonde-derived time series than that obtained *in situ*. A detailed calculation would be required to show what effect this might have on the cumulative probability distributions. Such an effect may be indicated by the data in figure 23. This analysis also suggests that the errors will be reduced as the echosonde pulse length is reduced, thus approaching the vertical sampling characteristics of the point sensor.

A similar treatment can be applied to the errors of the vertical echosonde relative to the tilted one. We define the following quantities for a horizontal, continuous turbulent layer:

$L_p = C\tau/2$,
L' = thickness of layer,
R = vertical range to scattering volume,
ϕ_0 = angle of tilted beam relative to the vertical,
ϕ_0' = angle of layer from the horizontal, and
Θ_0 = beam half-angle (e.g., to −6 dB power points).

These parameters are displayed in figure 29. The resulting error becomes, defining E_A as the error due to the geometrical aspect sensitivity (vertical echosonde/tilted echosonde) arising from the relative beamfilling,

$$E_A \approx \frac{2R \sin \Theta_0\ (\tan \phi_0 + \tan \phi_0')}{L_p} \qquad (11)$$

where $(\phi_0 + \phi_0')$ is the angle between the layer and the tilted beam. (This makes the error sensitive to the orientation of the instability-perturbed layer relative to that of the echosonde.) If we consider patches of small horizontal and vertical extent moving along an interface, the error becomes with $L' < L_p$:

$$E_A \approx \frac{2R \sin \Theta_0 \tan \phi_0}{L_p}. \qquad (12)$$

Taking $R = 100$ m, $5° < \Theta_0 < 10°$, $30° < \phi_0 + \phi'_0 < 40°$, and $L_p = 5$ m, we find $2 < E_A < 4$. This again is in the range of the errors observed. If the patches are inhomogeneously distributed along the layer, then a short time sample may produce highly variable results (e.g., as in fig. 20). The errors are also predicted to increase linearly with the height above the surface. However, the vertical distribution of C_T^2 may dominate such comparisons as in figure 22

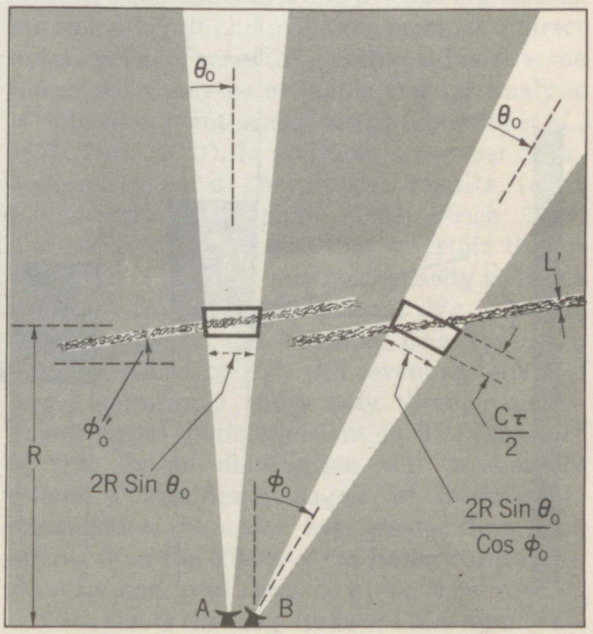

Figure 29. Schematic diagram for computation of the relative vertical echosonde/tilted echosonde error.

(cf., fig. 3). Since these errors are related to vertical inhomogeneity, a vertical averaging may reduce the variance of C_T^2 obtained from the vertically directed echosonde, but not the ratios of hourly averages as used in figure 22.

6. Summary & Conclusions

We have described the quantitative analysis of backscattered acoustic signals in the turbulent planetary-boundary layer. The acoustic measurements were obtained with two separate echosondes, one of which operated at simultaneous wavelengths of 0.12, 0.15, and 0.19 m. The measurements spanned the transition from a turbulence regime dominated by statie stability to one characterized by static instability.

The analysis utilized a cross section approximation in the echosonde equation. The acoustic scattering cross section was expressed in terms of an isotropic, three-dimensional temperature spectral density ϕ_T, evaluated at one-half the acoustic wavelength. For comparison of the observed echo with *in situ* data, ϕ_T was expressed in terms of the temperature structure function $D_T=[(\Delta T)^2]$ and equivalently in terms of C_T^2 assuming the "2/3 power law." ΔT was measured at a vertical separation of 0.20 m which was near the half wavelength of the acoustic waves being used.

Within a possible systematic experimental error of ±3 dB, the median echosonde C_T^2 agreed over a considerable range of conditions with the median *in situ* C_T^2. The cumulative probability distributions also agreed well, showing a lognormal character in most cases. Vertical profiles of C_T^2 followed the theoretically expected $Z^{-4/3}$ height-dependence under conditions of free convection, and inferences of the surface temperature flux from the echosonde agreed within the experimental error with values from the tower.

Under conditions of static stability, the vertical echosonde on occasion overestimated C_T^2 relative to the values from the tilted echosonde and the tower by factors ranging from 2 to 5. This report suggests that the quasi-horizontal spatial ordering of the small-scale turbulence structure under statically stable conditions may introduce averaging errors in the *in situ* C_T^2 measurements relative to the finite-volume echosonde measurements. The same spatial structure may introduce errors of the magnitude observed between the vertical echosonde and tilted one due to relative beamfilling effects. Our results suggest that such errors between the tower and the vertical echosonde values of C_T^2 are reduced by shortening the pulse length.

Our results thus show the ability of echosonde techniques (with the proper choice of beamwidth and pulse length) to yield a quantitative measure of the spectral density of temperature fluctuations at small scales under a variety of atmospheric conditions.

7.

Acknowledgments

The data that form the basis of this report were obtained through the efforts of many members of the WPL during the 1972 Haswell experiment. Dr. E. E. Gossard provided overall direction of the Haswell experiment and was responsible for the microbarograph data that aided the interpretation of our results. We are particularly indebted to G. R. Ochs who provided the *in situ* measurement of C_T^2. J. W. Wescott was responsible for the echosonde design and engineering that made reliable measurements possible. B. C. Willmarth obtained the transducer and antenna data from which the efficiencies were calculated and provided valuable technical assistance in obtaining the multifrequency data during the field operations.

The study itself was initiated by Dr. D. W. Beran using data from a 1969 experiment. These early results provided the major impetus for the 1972 experiment design. Numerous discussions with both Drs. Beran and F. F. Hall, Jr., Chief, Atmospheric Acoustics Program in WPL, and their support and encouragement have played a significant part in what success can be claimed for the present analysis.

Helpful comments by and conversations with many other members of WPL in the course of the analysis and in the preparation of this report are gratefully acknowledged.

We also acknowledge the partial financial support of the Rome (N.Y.) Air Development Center (U.S. Air Force Systems Command) and helpful comments by R. Urtz and D. Tarazano.

8. References

Batchelor, G. K. (1957), Wave scattering due to turbulence, in *Symposium on Naval Hydrodynamics, NAS-NRC Publ. 515,* F. S. Sherman, ed., National Research Council, Washington, D. C., pp. 409–430.

Battan, L. J. (1973), *Radar Observation of the Atmosphere,* Univ. of Chicago Press, Chicago, Ill., 324 pp.

Bean, B. R., and E. J. Dutton (1968), *Radio Meteorology,* Dover Publ. Inc., New York, N. Y., 435 pp.

Beran, D. W., W. H. Hooke, and S. F. Clifford (1973), Acoustic echo-sounding techniques and their application to gravity-wave, turbulence, and stability studies, *Boundary-Layer Meteorol. 4:* 133–153.

Browand, F. K., and C. D. Winant (1973), Laboratory observations of shear-layer instability in a stratified fluid, *Boundary-Layer Meteorol. 5:* 67–77.

Brown, E. H. (1974), Some recent NOAA theoretical work on echo sounding in the atmosphere, *J. Geophys. Res. 79:* 5567–5571.

Brown, R. A. (1974), *Analytical Methods in Planetary Boundary Layer Modelling,* John Wiley & Sons, New York, N. Y., 148 pp.

Busch, N. E., ed. (1973), Turbulence spectra at scales smaller than 1 meter, *Boundary-Layer Meteorol. 5:* 211–217.

Evans, E. J., and E. N. Bazley (1956), The absorption of sound in air at audio frequencies, *Acustica 6:* 238–245.

Frisch, A. S., and G. R. Ochs (1975), A note on the behavior of the temperature structure parameter in a convective layer capped by a marine inversion, *J. Appl. Meteorol. 14:* 415–419.

Gibson, C. H., G. R. Stegen, and R. B. Williams (1970), Statistics of the fine structure of turbulent velocity and temperature fields measured at high Reynolds number, *J. Fluid Mech. 41 (Pt. 1):* 153–167.

Gjessing, D. T., A. G. Kjelaas, and E. Golton (1973), Small-scale atmospheric structure deduced from measurements of temperature, humidity and refractive index, *Boundary-Layer Meteorol. 4:* 475–492.

Gossard, E. E., and W. H. Hooke (1975), *Waves in the Atmosphere,* Elsevier, Amsterdam, the Netherlands, 480 pp.

Gossard, E. E., D. R. Jensen, and J. H. Richter (1971), An analytical study of tropospheric structure as seen by high-resolution radar, *J. Atmos. Sci. 28:* 794–807.

Gossard, E. E., J. H. Richter, and D. R. Jensen (1973), Effect of wind shear on atmospheric wave instabilities revealed by FM/CW radar observations, *Boundary-Layer Meteorol. 4:* 113–131.

Gurvich, A. S., and A. M. Yaglom (1967), Breakdown of eddies and probability distributions for small-scale turbulence, *Phys. Fluids Suppl. 10 (Pt. II):* S59–S65.

Hall, F. F., Jr., and J. W. Wescott (1974), Acoustic antennas for atmospheric echo sounding, *J. Acoust. Soc. Am. 56:* 1376–1382.

Harris, C. M. (1966), Absorption of sound in air versus humidity and temperature, *J. Acoust. Soc. Am. 40:* 148–159.

Haurwitz, B. (1947), Internal waves in the atmosphere and convective patterns, *Ann. N. Y. Acad. Sci. 48:* 727–748.

Hooke, W. H., F. F. Hall, Jr., and E. E. Gossard (1973), Observed generation of an atmospheric gravity wave by shear instability in the mean flow of the planetary boundary layer, *Boundary-Layer Meteorol. 5:* 29–41.

Izumi, Y. (1964), The evolution of temperature and velocity profiles during breakdown of a nocturnal inversion and a low-level jet, *J. Appl. Meteorol. 3:* 70–82.

Kaimal, J. C., ed. (1969), Anisotropy of the fine structure, *Radio Sci. 4:* 1369–1370.

Kolmogorov, A. N. (1962), A refinement of previous hypothesis concerning the local structure of turbulence in a viscous incompressible fluid at high Reynolds number, *J. Fluid Mech. 13:* 82–85.

Kraichnan, R. H. (1953), The scattering of sound in a turbulent medium, *J. Acoust. Soc. Am. 25:* 1096–1104.

Kraichnan, R. H. (1966), Isotropic turbulence and inertial-range structure, *Phys. Fluids 9:* 1728–1752.

Lawrence, R. S., G. R. Ochs, and S. F. Clifford (1970), Measurements of atmospheric turbulence relevant to optical propagation, *J. Opt. Soc. Am. 60:* 826–830.

LeMone, M. A. (1973), The structure and dynamics of horizontal roll vortices in the planetary boundary layer, *J. Atmos. Sci. 30:* 1077–1091.

Lighthill, M. J. (1953), On the energy scattered from the interaction of turbulence with sound or shock waves, *Proc. Cambridge Phil. Soc. 49:* 531–551.

Little, C. G. (1969), Acoustic methods for the remote probing of the lower atmosphere, *Proc. IEEE 57:* 571–578.

McAllister, L. G., J. R. Pollard, A. R. Mahoney, and P. J. R. Shaw (1969), Acoustic sounding — A new approach to the study of atmospheric structure, *Proc. IEEE 57:* 579–587.

Metcalf, J. I., and D. Atlas (1973), Microscale ordered motions and atmospheric structure associated with thin echo layers in stably stratified zones, *Boundary-Layer Meteorol. 4:* 7–35.

Oboukhov, A. M. (1962), Some specific features of atmospheric turbulence, *J. Fluid Mech. 13:* 77–81.

Ottersten, H. (1970), Radar angels and their relationship to meteorological factors, *Swedish Res. Inst. Nat. Defense, FOA Repts. 4 (2),* Stockholm, Sweden, 33 pp.

Ottersten, H., K. R. Hardy, and C. G. Little (1973), Radar and sodar probing of waves and turbulence in statically stable clear-air layers, *Boundary-Layer Meteorol. 4:* 47–89.

Pao, Y. H. (1973), Measurements of internal waves and turbulence in two-dimensional stratified shear flows, *Boundary-Layer Meteorol. 5:* 177–193.

Simmons, W. R., J. W. Wescott, and F. F. Hall, Jr. (1971), Acoustic echo sounding as related to air pollution in urban environments, *NOAA Tech. Rept. ERL 216-WPL 17,* U. S. Govt. Printing Off., Washington, D. C., 77 pp.

Sutherland, L. C., ed. (1968), Sonic and vibration environments for ground facilities — A design manual, *Wyle Lab. Rept. No. WR-68-2,* NASA Contract NAS8-11217, Huntsville, Ala., chap. 7, pp. 1–14.

Tatarskii, V. I. (1961), *Wave Propagation in a Turbulent Medium* (R. A. Silverman, transl.), McGraw-Hill Book Co., Inc., New York, N. Y., 285 pp.

Tatarskii, V. I. (1971), *The Effects of the Turbulent Atmosphere on Wave Propagation* (Nauka, Moscow, 1967), transl. Israel Program for Scientific Translations, U. S. Dept. of Commerce, Nat. Tech. Inform. Serv., Springfield, Va., 472 pp.

Tennekes, H. (1973a), A model for the dynamics of the inversion above a convective boundary layer, *J. Atmos. Sci. 30:* 558–567.

Tennekes, H. (1973b), Intermittency of the small-scale structure of atmospheric turbulence, Part II, *Boundary-Layer Meteorol. 4:* 241–250.

Thorpe, S. A. (1973), Experiments on instability and turbulence in a stratified shear flow, *J. Fluid Mech. 61 (Pt. 4):* 731–751.

Tsvang, L. R. (1969), Microstructure of temperature fields in the free atmosphere, *Radio Sci. 4:* 1175–1177.

Wescott, J. W., W. R. Simmons, and C. G. Little (1970), Acoustic echo-sounding measurements of temperature and wind fluctuations, *ESSA ERLTM-WPL 5,* U. S. Dept. of Commerce, Boulder, Colo., 24 pp.

Wheelon, A. D. (1972), Backscattering by turbulent irregularities: A new analytical description, *Proc. IEEE 60:* 252–265.

Wyngaard, J. C., and O. R. Coté (1971), The budgets of turbulent kinetic energy and temperature variance in the atmospheric surface layer, *J. Atmos. Sci. 28:* 190–201.

Wyngaard, J. C., J. Izumi, and S. A. Collins, Jr. (1971), Behavior of the refractive-index-structure parameter near the ground, *J. Opt. Soc. Am. 61:* 1646–1650.

Appendix.

Echosonde Operation & Calibration

McAllister et al. (1969) and Simmons et al. (1971) describe the operational details of echosondes. In brief, a short pulse of acoustic energy with a given frequency or mixture of frequencies feeds a transducer mounted at the focus of an acoustically shielded parabolic antenna. This results in the propagation of an approximately plane wave pulse with an axisymmetric amplitude given by the gain pattern of a circular piston source. Measured gain patterns are shown in figure 30 over the available frequency range. Following the emission of the pulse, the system switches to a receive mode for a selected period before the next pulse. In this mode, the antenna collects and focuses the backscattered energy, giving a time and hence range-dependent voltage at the transducer output. Following swept-gain amplification (compensating the R^{-2} dependence of the scattered intensity), filtering, and rectification, this signal serves as an input to a facsimile recorder. Examples of four simultaneous multifrequency traces appear in figure 31. Parallel sequencing of such amplitude-modulated traces (at the pulse repetition rate of the echosonde) on the facsimile paper produces a time-height representation of the atmospheric structure moving through the beam. The unfiltered, filtered, and rectified signals are also recorded on a wide-band analog tape recorder for later quantitative analysis. The recording of the unfiltered signal from the preamplifier for later processing of both multifrequency and, in some operations, bistatic signal components, results in fewer requirements for supporting hardware during field operations.

Supporting meteorological data were obtained near the echosonde array, as shown in figure 1, from a 152-m tower instrumented at 30.5-m intervals. The instrumentation at these fixed levels and on the tower's movable carriage consisted of thermistors and bivanes. The 92-m

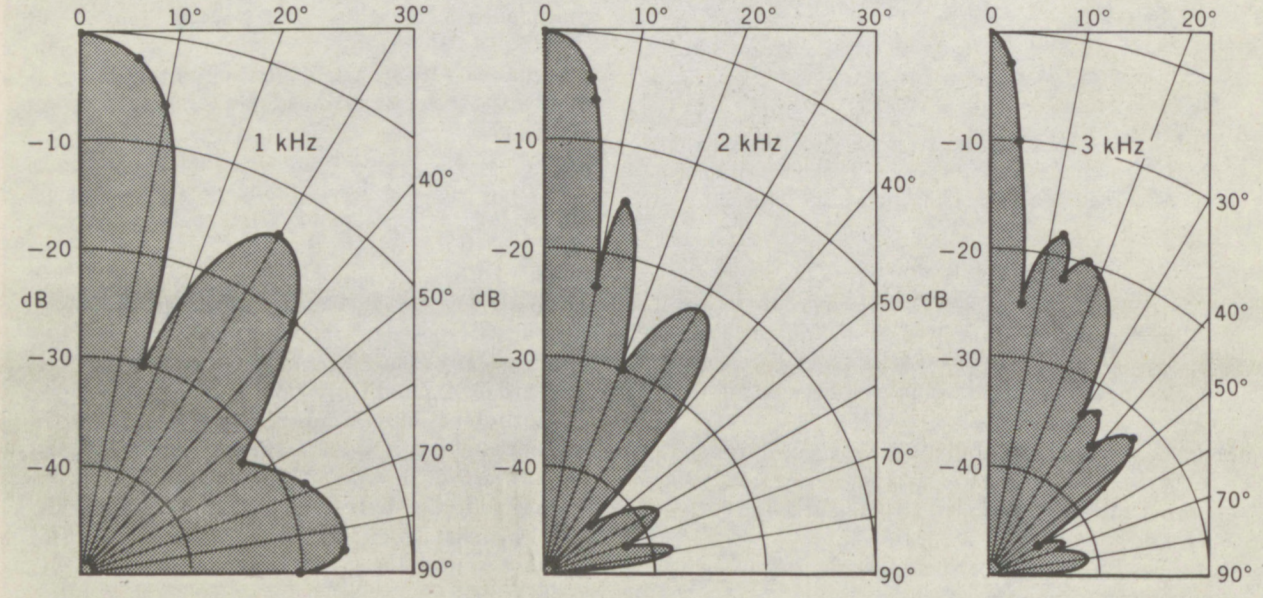

Figure 30. Antenna-gain patterns at 1000, 2000, and 3000 Hz.

tower level was instrumented with a "C_T^2 sensor" which gave, by analog computation, the rms-temperature difference between two fast-response sensors spaced 0.20 m apart in the vertical (Lawrence et al., 1970). These data were digitally recorded in 1-s integrated samples. In addition, hygrothermograph and barograph recordings were made at all the fixed levels and microwave refractivity at 61 and 92 m. These were used to calculate corrections for the attenuation of the acoustic signal as will be described later.

Application of the "echosonde equation" (1) and the expression (6) for the cross section yields a discrete time series of volume-averaged C_T^2 values for any selected echosonde range gate. The errors in the values of C_T^2 so determined depend to a large extent on one's ability to measure or estimate the correction terms in the echosonde equation. Once the total electronic gain of the system is accurately measured (within a few percent), the major error left in the evaluation of (1) for C_T^2 is that arising from estimates of the antenna-transducer efficiencies and to a lesser extent from the calculated attenuation. The transmit efficiency as a function of frequency was calculated from measurements of the sound pressure level produced at the aperture when a known power level was applied to the transducer. The receiving efficiency was measured by placing a sound source on axis, 10 m from the aperture, then regulating the pressure level at the aperture to 1 μbar as the source frequency was swept, and measuring the corresponding transducer power output. The results are shown in figure 32. There are errors of ± 2 dB inherent in this technique (Wescott et al., 1970), depending, for example, on whether the source is in the farfield of the antenna or whether the placement of the sound-level meter microphone gives an adequate indication of the average power produced. Additionally, figure 32 shows a frequency response that is not flat. In the transmit and receive modes, errors can be introduced as these apparently mechanical resonances shift with changing transducer temperature (usually in a diurnal pattern). In the receive mode, errors can be introduced by the variation in the frequency of the scattered signal caused by Doppler effects. These errors in the receive mode would be most prominent at higher frequencies and for tilted beam geometries. Of the three principal frequencies used, 1750, 2250, and 2750 Hz, the middle frequency can be seen from figure 32 to be the most reliable in this respect.[2]

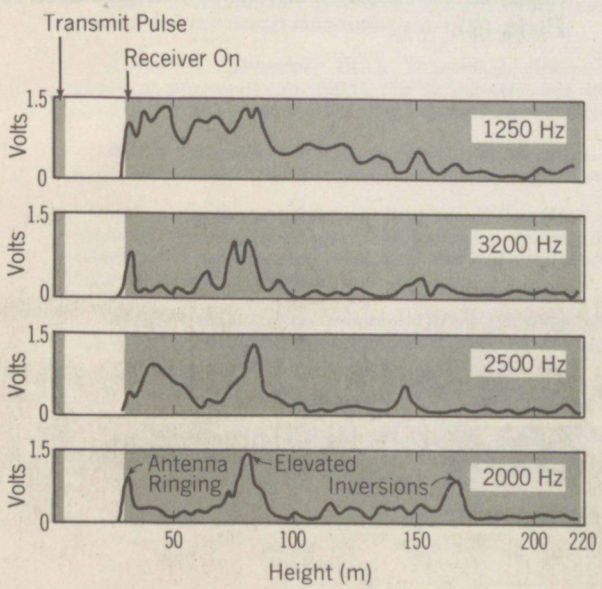

Figure 31. Simultaneous multifrequency returns.

There are also variations among individual transducers. Because only a simplified intercalibration procedure was utilized to check on these variations, there could be additional errors arising from the lack of the proper match with the actual antenna and atmosphere during these calibration measurements. The conclusion is that even though a probable error is not easily definable, one must contend with a possible error of several decibels. This type of error could be reduced through the design or selection of a transducer with a flatter frequency response.

The range-averaged attenuation $\bar{\alpha}$ is assumed to be equal to the sum of "classical absorption" (Evans and Bazley, 1956) and molecular absorption (Harris, 1966). Classical absorption α_{cl} arises from the effects of heat conduction and viscosity and is generally small. Molecular absorption α_{mol} is larger, arising from the excitation by the sound wave of the internal energy modes of gases such as O_2 in the atmosphere (through local increases in the collision rate). The water vapor content of the air strongly influences this excitation process and hence becomes the important factor in the

[2]For mixed-frequency operation, a mechanical transfer of energy between frequencies is possible within the transducer. For our choice of frequencies, this possibility was examined and found not to be a significant problem. For operational situations, the efficiencies ought to be measured or inferred using mixed frequencies in the calibration procedure.

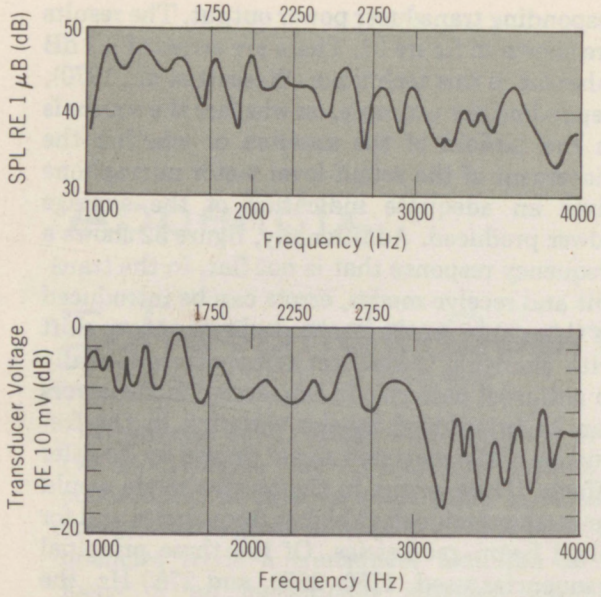

Figure 32. (a) Sound pressure level (SPL) at the antenna aperture when 10 W (electrical) were applied to the transducer; and (b) transducer voltage output when 1-μbar rms-pressure was applied at the antenna aperture.

calculation of α_{mol}. Sutherland (1968) gives a detailed discussion of these processes and empirically fits equations that allow a straightforward calculation of $\bar{\alpha}=\bar{\alpha}_{cl}+\bar{\alpha}_{mol}$. The calculation of α_{mol} is in terms of a frequency f_m at which maximum absorption occurs that is also a function of temperature (T, °C) and atmospheric pressure (P, mb) and is given empirically by

$$f_m=(10+6600\,h+44{,}400\,h^2)\,P^*/(T^*)^{0.8}\,Hz$$

where h = percent mole ratio of water vapor $=100\cdot\frac{e}{P}$ where e = water vapor pressure (mb),

T^* = [1.8 (T°C)+492]/519, and

P^* = P/1014.

This then defines the maximum absorption (at frequency f_m)

$$\alpha_{max}=0.0078\,f_m\cdot(T^*)^{-2.5}\,e^{7.77(1-T^{*-1})},$$

whence α_{mol} is

$$\alpha_{mol}=\frac{\alpha_{max}}{304.8}\left\{\left[0.18\frac{f}{f_m}\right]^2+\left[\frac{2(f/f_m)^2}{1+(f/f_m)^2}\right]^2\right\}^{1/2}\left(\frac{-dB}{m}\right)$$

where f = echosonde-operating frequency (H_z). α_{cl} has a weak dependence on temperature and is approximated by Sutherland as

$$\alpha_{cl}=1.74\times10^{-10}\,f^2\,(-dB/m).$$

We calculated $\bar{\alpha}$ by using hourly averages of water vapor pressure, temperature, and pressure derived from hygrothermograph and barograph recordings at the 31-, 61-, 92-, and 152-m tower levels, converted to attenuation per meter, linearly interpolated, and range-averaged for use in (1). The effects of short-term variations in humidity were estimated from the 61-m level microwave-refractivity measurements (N) and found to produce less than 5-percent variation in the final calculation of C_T^2. These were calculated from $N=77.6\,P/T+3.73\times10^5\,e/T^2$ (Bean and Dutton, 1968). For the experiment at hand, the air was quite moist from recent rains and the associated ground moisture. Hence, because of the large value of f_m, little variation was produced in the calculation of α_{mol}. For drier air, where the attenuation becomes more sensitive to the water vapor content, greater care would have to be exercised when applying this correction.

The calculation of the "effective-aperture factor" G (Hall and Wescott, 1974) is sensitive to the assumed distribution of scatterers and hence to the integration over the beam-gain pattern. A factor of 0.40 is used. This is consistent with other estimates of the "effective aperture" of antennas (Little, 1969; Battan, 1973).

The remaining terms in (1) are either directly measured or estimated from the system parameters. One should note that the open-circuit voltage v_R at the transducer is measured in the receive mode. If the transducer were terminated by its characteristic impedance Ω, then the maximum power transferred would be $(v_R/2)^2/\Omega$ (Wescott et al., 1970) which is used for P_R in (1).

☆ U.S. GOVERNMENT PRINTING OFFICE: 1974 — 677-241/1270 REGION NO. 8

ENVIRONMENTAL RESEARCH LABORATORIES

The mission of the Environmental Reasearch Laboratories is to study the oceans, inland waters, the lower and upper atmosphere, the space environment, and the earth, in search of the understanding needed to provide more useful services in improving man's prospects for survival as influenced by the physical environment. Laboratories contributing to these studies are:

Atlantic Oceanographic and Meteorological Laboratories (AOML): Geology and geophysics of ocean basins and borders, oceanic processes, sea-air interactions and remote sensing of ocean processes and characteristics (Miami, Florida).

Pacific Marine Environmental Laboratory (PMEL): Environmental processes with emphasis on monitoring and predicting the effects of man's activities on estuarine, coastal, and near-shore marine processes (Seattle, Washington).

Great Lakes Environmental Research Laboratory (GLERL): Physical, chemical, and biological, limnology, lake-air interactions, lake hydrology, lake level forecasting, and lake ice studies (Ann Arbor, Michigan).

Atmospheric Physics and Chemistry Laboratory (APCL): Processes of cloud and preciptation physics; chemical composition and nucleating substances in the lower atmosphere; and laboratory and field experiments toward developing feasible methods of weather modification.

Air Resources Laboratories (ARL): Diffusion, transport, and dissipation of atmospheric contaminants; development of methods for prediction and control of atmospheric pollution; geophysical monitoring for climatic change (Silver Spring, Maryland).

Geophysical Fluid Dynamics Laboratory (GFDL): Dynamics and physics of geophysical fluid systems; development of a theoretical basis, through mathematical modeling and computer simulation, for the behavior and properties of the atmosphere and the oceans (Princeton, New Jersey).

National Severe Storms Laboratory (NSSL): Tornadoes, squall lines, thunderstorms, and other severe local convective phenomena directed toward improved methods of prediction and detection (Norman, Oklahoma).

Space Environment Laboratory (SEL): Solar-terrestrial physics, service and technique development in the areas of environmental monitoring and forecasting.

Aeronomy Laboratory (AL): Theoretical, laboratory, rocket, and satellite studies of the physical and chemical processes controlling the ionosphere and exosphere of the earth and other planets, and of the dynamics of their interactions with high-altitude meteorology.

Wave Propagation Laboratory (WPL): Development of new methods for remote sensing of the geophysical environment with special emphasis on optical, microwave and acoustic sensing systems.

Marine EcoSystem Analysis Program Office (MESA): Plans and directs interdisciplinary analyses of the physical, chemical, geological, and biological characteristics of selected coastal regions to assess the potential effects of ocean dumping, municipal and industrial waste discharges, oil pollution, or other activity which may have environmental impact.

Weather Modification Program Office (WMPO): Plans and directs ERL weather modification research activities in precipitation enhancement and severe storms mitigation and operates ERL's research aircraft.

NATIONAL OCEANIC AND ATMOSPHERIC ADMINISTRATION
BOULDER, COLORADO 80302